ORIGINAL ARTICLE

lajss.org© Latin American Journal of Solids and Structures

www.lajss.org

Fragmentation model for the tensile response of unidirectional composites based on the critical number of fiber breaks and the correction of the fiber-matrix interfacial strength.

Juan David Vanegas-Jaramillo[a,b*]

Iván David Patiño-Arcila[a,c]

[a] Grupo de Investigación en Nuevos Materiales (GINUMA), Universidad Pontificia Bolivariana, Medellín, Colombia.
E-mails: jdvanegasj@gmail.com, i.patinoar@pascualbravo.edu.co
[b] Grupo de Investigación en Materiales Avanzados y Energía (MAtyER), Instituto Tecnológico Metropolitano, Medellín, Colombia.
[c] Grupo de Investigación e Innovación Ambiental (GIIAM), Instituto Tecnológico Pascual Bravo, Medellín, Colombia.

* Corresponding Author

http://dx.doi.org/10.1590/1679-78255326

Abstract

A fragmentation model based on global load sharing (GLS) theory is developed to obtain stress-strain curves that describe the mechanical behavior of unidirectional composites. The model is named $CNB + \tau^*$ because it is based on the Critical Number of Breaks model (CNB) and on the correction of the fiber matrix interfacial strength, τ^*. Model allows both obtaining the ultimate tensile strength of CFRP and GFRP composites, and correcting the σ vs ε curve to match its peak point with the predicted strength, which is more accurate than the one obtained by previous GLS-based models. Our model is used to classify the mechanical response of the material according to the energetic contributions of two phenomena up to the failure: intact fibers (IF) and fragmentation (FM). Additionally, the influence of fiber content, V_f, on the tensile strength, σ_U, failure strain, ε_U, and total strain energy, U_T, is analyzed by means of novel mechanical-performance maps obtained by the model. The maps show a dissimilar behavior of σ_U, ε_U and U_T with V_f between GFRP and CFRP composites. The low influence of V_f on the percent energetic contributions of IF and FM zones, as well as the larger energetic contribution of the FM zone, are common conclusions that can be addressed for both kinds of composites.

Keywords

Polymer matrix composites, stress-strain behavior, fragmentation model, critical number of breaks, fiber-matrix interfacial strength

1 INTRODUCTION

Most of the analytical models used to predict the mechanical behavior of unidirectional composite materials consider the stochastic representation of the occurrence of fiber breakings. They are based on the fragmentation theory and global load sharing (GLS) approach, and can be considered useful tools to assist the mechanical design of composite materials (Lamon 2010). Fragmentation modeling is critical for the determination of the mechanical response of composite materials, as well as for the estimation of the stress-strain response (Lamon 2010). Curtin was the first to develop a law of fragmentation from an expansion of Taylor series that allow approximating the Weibull function, obtaining analytical solutions for the curve σ vs ε (Curtin 1991a, 1991b). This model was later extended by Neumeister to roughly explain the superposition of the zones of influence adjacent to the fiber breaks (Neumeister 1993a, 1993b). On the other hand, Hui et al. (Hui et al. 1995) obtained the governing equations for a problem of fiber fragmentation,

Received: October 17, 2018. In Revised Form: July 21, 2019. Accepted: July 22, 2019. Available online: July 23, 2019.
http://dx.doi.org/10.1590/1679-78255326

Latin American Journal of Solids and Structures. ISSN 1679-7825. Copyright © 2019. This is an Open Access article distributed under the terms of the Creative Commons Attribution License, which permits unrestricted use, distribution, and reproduction in any medium, provided the original work is properly cited.

however, these cannot be solved analytically, and can only be evaluated numerically. In addition, Turon et al. developed a progressive damage model for unidirectional composite laminates, capable of accounting for the loss of stiffness due to the separation of the reinforcement on the vicinity of the fiber rupture (Turon et al. 2005). The main differences between these works lie in the consideration or not of phenomena such as fiber pull-out, sliding, fiber separation and/or the distribution of the global or local load after breakage, which entail different mathematical complexity. Consequently, the mentioned models show moderate differences in the relation σ vs ε before the peak point of the curve, and important dissimilarities from that point onwards.

The model developed by Neumeister includes a refined constitutive law to predict the tensile behavior of brittle materials in terms of a damage variable, without solving differential equations or evaluating auxiliary functions numerically (Neumeister 1993a). The Neumeister model has several similarities with the work done by Curtin (Curtin 1991a, 1991b), however, Neumeister model is much simpler and can offer a more accurate solution (Neumeister 1993a). The Neumeister equation is given by:

$$\sigma_{\infty_{Neum}} = V_f \cdot \sigma_f \left[\frac{1}{w+1} + \frac{1}{2 \cdot ln(w+1)} \left(\frac{w}{w+1}\right)^2\right] \tag{1}$$

where V_f is the fiber volume content and w is a damage variable that depends on the fiber stress, σ_f , the critical stress, σ_c, and the Weibull modulus, β, as given by:

$$w = \left(\frac{\sigma_f}{\sigma_c}\right)^{\beta+1} \tag{2}$$

Even though the stress-strain behavior predicted by GLS-based models reasonably agrees with experimental tests for low density of fiber breaks, the ultimate tensile strength predicted by these models significantly differs from experimental values. In general, the GLS-based models considerably overpredict the tensile strength because they do not consider the stress concentration factor around the breaks (Swolfs et al. 2015). In general, when a fiber break occurs, the load released is redistributed among the intact adjacent fibers in order to obtain a local load equilibrium. The stress is intensified in the neighboring fibers, increasing their probability to fracture. The way in which the concentration factor that accounts for the stress redistribution in the fibers surrounding the break is computed determines the accuracy of the predicted strength. There exist some numerical models that consider the stress concentration around the broken fibers and are usually named Local Load Sharing (LLS) models (Beyerlein and Phoenix 1996b; Ibnabdeljalil and Curtin 1997; Sastry and Phoenix 1993; Zhou and Curtin 1995). They make use of complex mathematical formulations (Harlow and Phoenix 1978a, 1978b) or numerical Monte-Carlo Simulations (Curtin and Takeda 1998a, 1998b; Landis, Beyerlein, and McMeeking 2000; Okabe et al. 2001), which increase the computational cost. Generally speaking, LLS models tend to underpredict the composite strength (Behzadi, Curtis, and Jones 2009).

Accordingly, the traditional GLS-based models, as the Neumeister one, are very useful since they provide fast and accurate results about the stiffness of the composite in the linear elastic zone, but their main drawback lies in the over-prediction of the ultimate tensile strength of the composite. Bearing this in mind, Koyanagi et al. (Koyanagi et al. 2009) presented the Simultaneous Fiber-Failure (SFF) model, which assumes that the unidirectional composite fails when a certain number of simultaneous fiber breaks, *n,* occur. This critical number of fiber breaks was estimated from the experimental strength of different composite materials. Then, for the composite materials considered, a phenomenological relationship was established between the fiber breaks, *n,* and the strength ratio, $\tau/\sqrt{\sigma_0 \sigma_m}$, where τ is the fiber-matrix interfacial strength, σ_0 is the characteristic stress of the Weibull distribution and σ_m is the strength of the matrix. Koyanagi et al. mixed different material systems such as glass and carbon fiber-reinforced polymeric composites (GFRP and CFRP, respectively), ceramic matrix composites (CMC), and carbon/carbon composites (C/C). Although their predictions of the ultimate tensile strength were reasonably accurate for C/C and CMC, the same conclusion could not be addressed for GFRP and CFRP. Thereby, it can be asserted that the Koyanagi's GLS-based model is not particularly suitable for CFRP and GFRP composites. Recently, Lamus, Linero and Guevara presented a two-dimensional numerical model able to describe the fracture process in structural members of steel fibre reinforced concrete (SFRC) in terms of the fiber volume ratio and the mechanical properties of the components (Augusto 2019). Mixture theory was used for the stress-strain relationship; concrete matrix was represented with a scalar damage constitutive model; one-dimensional plasticity constitutive model was employed for fibers and fiber-matrix interface; the jumps in the displacement field and corresponding non-bounded values of strains, which are associated to cracking, were represented using a Continuum Strong Discontinuity Approach; non-linear finite element analysis was implemented

to solve the governing equations of the model, and a bootstrap stochastic methodology was used to establish confidence intervals for the structural response considering that reinforcements are short fibers randomly oriented and distributed. The model can be considered suitable in the sense that most of experimental results of Load vs. Displacement for tensile and bending tests of SFRC beams lies in the predicted confidence intervals, but that model is not conceived to predict the exact mechanical response of continuous and oriented fiber-reinforced composites, as the one proposed here. Another work dealt with the toughening effect produced by the fibers at the early stage of a crack formation (Wang and Friedrich 2013), which consists on the increase of stress of fibers in the neighborhood of an initial crack in order to keep the two opening surfaces of the crack from separating. Influence of fiber strength, fiber-matrix interface resistance, fiber diameter and elasticity modulus on the percentage of effective fibers were evaluated, finding that the lower the elasticity modulus and the higher the fiber strength, the larger the toughening effect. Not quantitative comparison with experiments were carried out in that work since not experimental data of effective fibers around initial cracks are available in the literature. The mentioned work focused on the simulation of a phenomenon arising in the initial crack, i.e, toughening, but not on the whole damage process of the composite.

Damage progression of composite materials can be considered by using macroscopic models as well. For instance, Ghannadpour and Shakeri used the Hashin failure criteria and proposed a material degradation model to predict the failure and progressive damage behavior of composites plates containing initial geometric imperfections, when subjected to in-plane compressive loads (Ghannadpour and Shakeri 2018). A collocation method was used by the authors, where domain was discretized with Legendre-Gauss-Lobato nodes and displacement field was approximated by Legendre Basis Functions. The ply-by-ply failure and damage progression of the laminate was estimated in that work, but the accuracy of the results showed to be very sensible to the plate thickness and area of region around the location of failure. Progressive failure and finite element methods have been combined in several works to predict the stress-strain behavior of composites structures at macroscopic level. Average stress-average strain curves for compressive loads have been obtained by these methods in stiffened curved panels using Tsai-Wu criterion (Chen and Guedes Soares 2007), grid stiffened composite plates/shells using modified Hashin criterion (Zhang, Chen, and Ye 2008) and laminated shell structures using the extended Hashin criterion (Wagner and Balzani 2010). In a similar fashion, Morshedsolouk and Khedmati obtained the average stress-average strain curves of composite ships' stiffened panels to study the buckling and post-buckling behavior of these panels in terms of the aspect ratio, initial geometrical imperfection and stiffener size, using the Tsai-Wu failure criterion (Morshedsolouk and Khedmati 2014). These curves are very useful for comparative and parametric analysis purposes, but the predicted ultimate strength can considerably differ from experimental results since the phenomena involved in the damage process are not explicitly considered at microscopic level, as in the present work. In another work, the Extended Finite Element Method (XFEM) and 3D Puck´s failure theory were used to evaluate the crack evolution in thick composites structures (Angelo, Ribeiro, and Tita 2018), obtaining satisfactory results for thick laminated composites with layers oriented to 90˚ that undergo translaminar failure. In addition, compact tension tests with 0°, 90° and 45° specimens were evaluated, and numerical results were qualitatively coherent with experimental data.

In a previous work (Vanegas-Jaramillo et al. 2018), we reformulated the Neumeister and Turon models, which are based on the Global Load Sharing approach, with the purpose to predict accurately the tensile strength of unidirectional composite materials in terms of the number of breaks per unit length, Λ. It was proposed that the failure of the composite occurs when a critical number of breaks per unit length is reached; this critical break density depends on the constituent properties and the fiber volume content of the composite. In the model, called the Critical Number of Break model (CNB), an empirical law for the critical number of breaks as a function of the overall fragmentation limit stress and the volumetric fiber content, was deduced taken into account data of carbon fiber and glass fiber reinforced polymers (CFRP and GFRP, respectively) obtained from the literature. The CNB model implied an improvement of the GLS-based fragmentation models, with the ability to predict accurately the tensile strength of CFRP and GFRP composites. In general, the peak point of the σ vs ε curves obtained by Neumeister and Turon models does not match with the tensile strength computed with CNB (see Figure 1).

The value of tensile strength predicted by the CNB model is lower than the one obtained by the original Neumeister and Turon models, which implies that the overall stress-strain response of the composite should be different as well. In other words, the relocation of the failure point in the original Neumeister or Turon stress-strain curve, according to the value predicted by CNB, cannot be considered a satisfactory strategy since the stress-strain response is not fully linear up to failure, but instead, a non-linear response is appreciated at the end of the damage process due to the arising of the fiber fragmentation phenomenon (See Figure 1). The main purpose of the present work is to obtain stress-strain curves that describes more accurately the real behavior of the composite according to the tensile strength predicted by CNB. The effect of several micro-mechanical variables on the global stress-strain response is analyzed, finding that the

variation of the fiber-matrix interfacial strength, τ, allows 'contracting' or 'expanding' the curve keeping constant the initial slope (the Young modulus of the composite), which in turns entails the relocation of the peak point of the curve. A numerical procedure is developed to find the corrected fiber-matrix interfacial strength, τ^*, that brings about a good agreement between the peak point of the curve σ vs ε and the ultimate tensile strength predicted by CNB.

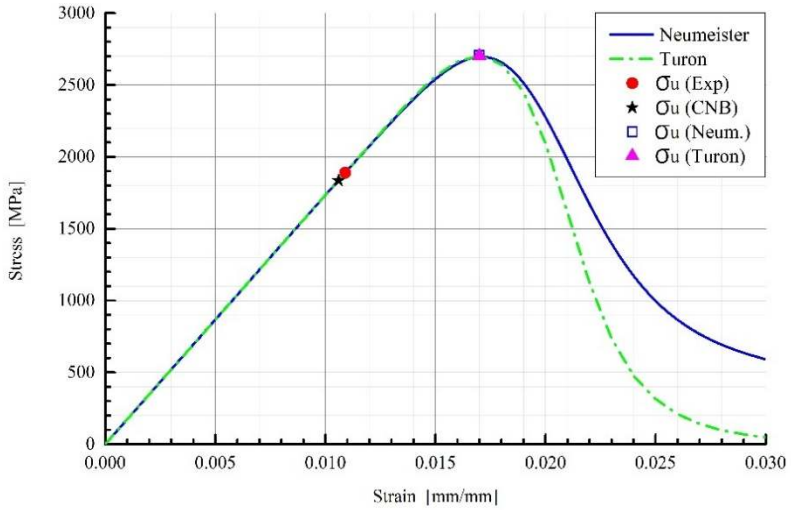

Figure 1: Predicted and experimental mechanical response for typical carbon/epoxy composite using Neumeister's, Turon's and CNB models

On the other hand, in the present work, the process of damage of the composite is divided into different phenomena. At the beginning, the reinforcement offers a linear elastic behavior and the fibers are intact (IF). If the load is increased, the defects act as stress concentrators where cracks arise along the fibers, and this phenomenon is called fragmentation (FM). The fragmentation evolves until the crack saturation in the fibers occurs, moment from which the fibers cannot be longer fragmented, and the material starts developing the sliding/separation phenomenon (SS). In this work, it was estimated the energetic contribution of these phenomena in the curve $\sigma\ vs\ \varepsilon$ of both CFRP and GFRP composites. Results showed that the fragmentation phenomenon of the fibers (FM) has the largest energetic contribution during the damage process. In this point, it is worth-mentioning that previous works has introduced damage estimators as a function of the strain energy. For instance, Gillich et al. expressed the damage severity produced by cracks located in a cantilever, multi-layered beam as a function of the stored energy, in order to study the influence of the crack depth on the natural frequency ship at several longitudinal positions of the beam (Gillich et al. 2016). Accurate results were obtained in that work for some vibration modes when compared to experiments. In general, strain energy can be considered an acceptable parameter to account for the damage evolution; in the present case, it is used to discriminate the different phenomena involved in the stress-strain response of the composite, namely, linear elastic behavior (IF), fragmentation (FM) and sliding/separation (SS).

In order to assist the design of structural composites, we propose mechanical-performance-maps that allow analyzing the influence of the fiber content, V_f, on the tensile strength, σ_U, failure strain, ε_U, and total strain energy, U_T, of the composite. In this way, by knowing the constituent properties of the CFRP and GPRP considered here, and the fiber volume content, V_f, these maps are useful to estimate the mechanical response of the material and classify the energetic contributions during the damage process. The fragmentation model proposed here is named $CNB + \tau^*$, and can be considered a valuable tool to predict the stress-strain behavior of unidirectional composites with good accuracy.

2 MODELING OF THE MECHANICAL RESPONSE

2.1 Critical Number of Breaks Model (CNB)

According to the Critical Number of Breaks model (CNB), the ultimate strength corresponds to a critical density of fiber breaks that are proper of the material (Vanegas-Jaramillo et al. 2018). Once this critical density of breaks has been reached, the fracture of the composite occurs; in this point, the interaction between fiber breaks becomes important enough to create 'avalanche events' of broken fibers that lead to the failure of the material. In the CNB model, it was introduced the overall fragmentation limit stress, σ_c', which relates the constituent properties and the fiber volume

content of unidirectional composites. This stress σ_c' can be defined as the remote stress that, on average, causes the crack saturation in all fibers of the composite. That is, once this stress level is reached, the composite is not able to develop further fragmentation, and other damage mechanisms, such as fiber sliding and separation, arise. Consequently, the critical number of breaks per unit length (Λ_{C}) and the overall fragmentation limit stress (σ_C') correspond to the same loading state of the composite, i.e., the moment where the fiber fragmentation stops. In a previous work (Vanegas-Jaramillo et al. 2018), for a set of ten different materials, it was shown that the behavior of Λ_{C} with σ_C' is different between CFRP and GFRP composites. For CFRP, Λ_{C} increases with σ_C', whereas for GFRP composites, this decreases. In that study, it was obtained a fitting relationship between these two variables, Λ_{C} and σ_C', as given by:

$$\Lambda_{\mathrm{C}} = e^{a\cdot(\sigma_C')^2+b\cdot(\sigma_C')+c} \tag{3}$$

where the parameters a, b and c depends on the composite and correspond to the coefficients of a second order polynomial fitting for the relation $\ln\Lambda_{\mathrm{C}}$ vs σ_C' (See Table 1).

Table 1: Estimation of the parameters of the Critical Number of Breaks model (CNB) for carbon and glass fiber reinforced composites

	Coefficient		
	a	***b***	***c***
CFRP	-3.21E-8	1.35E-4	-16.06
GFRP	3.613E-9	-2.36E-5	0.903

In the CNB model, the Neumeister curve can be posed in terms of the number of breaks per unit length or break density, Λ, as follows (Vanegas-Jaramillo et al. 2018):

$$\sigma_{CNB} = V_f \cdot (\Lambda\, L_0)^{\frac{1}{\beta}} \cdot \sigma_0 \cdot \left[\frac{1}{(2L_t\cdot\Lambda)+1} + \frac{1}{2\cdot ln\left((2L_t\cdot\Lambda)+1\right)}\left(\frac{(2L_t\cdot\Lambda)}{(2L_t\cdot\Lambda)+1}\right)^2\right] \tag{4}$$

Consequently, the ultimate tensile strength of a GFRP or CFRP composite can be obtained by computing first the overall fragmentation limit stress, σ_c', and, then, the critical number of breaks per unit length, Λ_{C}. The first parameter takes into account the level of stress that entails to the fragmentation of all fibers, and it is equivalent to:

$$\sigma_C' = \frac{\sigma_C}{V_f} \tag{5}$$

where σ_C is called the critical stress, which is computed as follows:

$$\sigma_c = \sigma_0 \left(\frac{2\cdot L_o\cdot\tau}{d\cdot\sigma_0}\right)^{\frac{1}{\beta+1}} \tag{6}$$

and V_f is the fiber volume content of the composite. In (6), σ_0 is the characteristic stress, L_o is the characteristic length, τ is the fiber-matrix interfacial strength, d is the fiber diameter, and β is the Weibull modulus of the fiber. Once the overall fragmentation limit stress, σ_C', has been obtained, it is possible to calculate the critical number of breaks, Λ_{C}, by using (3). Then, the value of Λ_{C} is substituted into (4) to compute the ultimate tensile strength of the composite, which can be represented as σ_{CNB}. One of the goals of the present work is to determine which of the microscopic parameters intervening in the Neumeister model is able to 'contract' the stress-strain curve in such a way that the peak point of this curve coincides with the ultimate tensile strength predicted by our CNB model, σ_{CNB}.

2.2 Determination of the ultimate strain and tensile strength of the composite.

The Neumeister model was previously defined in (1). That equation was presented in terms of the damage variable, w, which in turn is defined by (2). By using the Hooke´s law in the fibers, i.e., $\sigma_f = E_f\varepsilon$, the damage variable can be expressed as follows:

$$w = \Upsilon \cdot \varepsilon^{\kappa} \tag{7}$$

where $\Upsilon = \left(E_f/\sigma_c\right)^{\kappa}$, $\kappa = \beta + 1$, σ_c is the critical stress and β is the Weibull modulus. By substituting (7) into (1), the Neumeister equation in terms of the strain arises, as given by:

$$\sigma_{\infty Neum} = \varepsilon \cdot \eta \cdot \left[\frac{1}{\Upsilon.\varepsilon^{\kappa}+1} + \frac{1}{2\cdot\ln(\Upsilon\cdot\varepsilon^{\kappa}+1)} \cdot \left(\frac{\Upsilon\cdot\varepsilon^{\kappa}}{\Upsilon\cdot\varepsilon^{\kappa}+1}\right)^2\right] \tag{8}$$

where $\eta = V_f \cdot E_f$. The first and second terms in the brackets in (8) can be called the function of intact fibers, $G(\varepsilon)$, and the function of sliding/separation of fibers, $H(\varepsilon)$, respectively. Thereby, those functions are defined in terms of the strain, ε, as follows:

$$G(\varepsilon) = \frac{1}{\Upsilon\cdot\varepsilon^{\kappa}+1} \tag{9}$$

$$H(\varepsilon) = \frac{1}{2\cdot\ln(\Upsilon\cdot\varepsilon^{\kappa}+1)} \cdot \left(\frac{\Upsilon\cdot\varepsilon^{\kappa}}{\Upsilon\cdot\varepsilon^{\kappa}+1}\right)^2 \tag{10}$$

Taking into account the functions given in (9) and (10), the equation (8) can be represented as:

$$\sigma_{\infty Neum} = \varepsilon \cdot \eta \cdot \left[G(\varepsilon) + H(\varepsilon)\right] \tag{11}$$

In general, the stress-strain response of the composite obeys to several phenomena. For small deformations, the material behavior is linear elastic and no cracks are present in the fibers. The linear elastic behavior of the material ceases when cracks appear in the fibers. From that point until the peak point of the curve $\sigma\ vs.\ \varepsilon$, several cracks arise in the fibers until the maximum saturation of cracks has been achieved. Once the peak of the curve has been reached, the fiber fragmentation stops and the fiber sliding and separation become the predominant phenomena, which brings about the decrease of the global response of the stress with the strain. The last analysis allows concluding that the Neumeister curve only has a global maximum point, which can be obtained by setting the derivative of (11) with respect to ε to zero, as given by:

$$\frac{\partial\sigma_{\infty Neum}}{\partial\varepsilon} = \eta \cdot \left[G(\varepsilon) + H(\varepsilon)\right] + \eta \cdot \varepsilon \left[\frac{\partial G(\varepsilon)}{\partial\varepsilon} + \frac{\partial H(\varepsilon)}{\partial\varepsilon}\right] = 0 \tag{12}$$

where:

$$\frac{\partial G(\varepsilon)}{\partial\varepsilon} = -\frac{\Upsilon\cdot\kappa\cdot\varepsilon^{\kappa-1}}{(\Upsilon\cdot\varepsilon^{\kappa}+1)^2} \tag{13}$$

$$\frac{\partial H(\varepsilon)}{\partial\varepsilon} = -\frac{\Upsilon^3\cdot\kappa\cdot\varepsilon^{3\kappa-1}}{2(\Upsilon\cdot\varepsilon^{\kappa}+1)^3\cdot(\ln(\Upsilon\cdot\varepsilon^{\kappa}+1))^2} - \frac{\Upsilon^3\cdot\kappa\cdot\varepsilon^{3\kappa-1}}{(\Upsilon\cdot\varepsilon^{\kappa}+1)^3\cdot\ln(\Upsilon\cdot\varepsilon^{\kappa}+1)} + \frac{\Upsilon^2\cdot\kappa\cdot\varepsilon^{2\kappa-1}}{(\Upsilon\cdot\varepsilon^{\kappa}+1)^2\cdot\ln(\Upsilon\cdot\varepsilon^{\kappa}+1)} \tag{14}$$

The value of the strain ε that satisfies (12), can be considered as the ultimate strain of the composites, $\varepsilon_{ultimate}$, since the loading support capacity ceases from such point onwards. Consequently, the ultimate tensile strength, $\sigma_{ultimate}$, can be obtained by evaluating (11) in $\varepsilon = \varepsilon_{ultimate}$, leading to:

$$\sigma_{ultimate} = \varepsilon_{ultimate} \cdot \eta \cdot \left[G(\varepsilon_{ultimate}) + H(\varepsilon_{ultimate})\right] \tag{15}$$

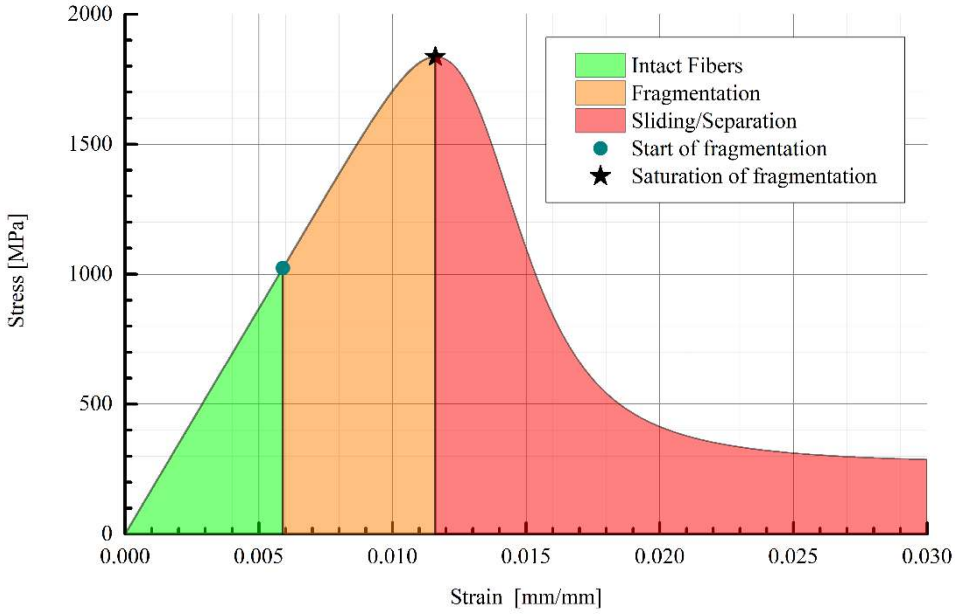

Figure 2: Identification of the principal phenomena in the σ vs. ε curve

2.3 Decomposition of the mechanical response of σ vs. ε curve by physical phenomena

The curve $\sigma\ vs\ \varepsilon$ obtained from equation of Neumeister, (1), can be decomposed into several zones that account for the phenomena involved in the damage process of the composite as the deformation increases (Figure 2). These phenomena are represented in the 'softening' terms of the Neumeister equation, which correspond to the two terms in brackets in equation (11), namely, the function of intact fibers, $G(\varepsilon)$, and the function of sliding/separation, $H(\varepsilon)$. In the elastic zone, the Hooke´s law is valid and the function of intact fibers, $G(\varepsilon)$, is practically one, whereas the sliding/separation function, $H(\varepsilon)$, is almost zero. When $G(\varepsilon) < 0.999$ approximately, the fiber fragmentation process starts. As long as the length of the fiber fragments is larger than a critical length, l_c, the fiber fragmentation is still possible and smaller portions are continuously generated; however, when this length is lower than l_c, the crack saturation occurs and, almost immediately, the sliding/separation function, $G(\varepsilon)$, becomes significant, which means that fibers are not able to break anymore in smaller portions, leading to the sliding and separation of the fibers.

The Neumeister curve $\sigma\ vs\ \varepsilon$ of a typical CFRP composite, whose properties are shown in Table 2, is represented in Figure 2. In that curve, three zones can be clearly identified: zone of intact fibers (*green zone*), zone of fragmentation (*orange zone*) and zone of sliding/separation (*red zone*). The area of each zone represents the internal strain energy per unit volume, in such a way that in that case, of the total energy, 13% corresponds to the intact-fiber phenomenon, 36% to fragmentation and 51% to sliding/separation. If the curve is only analyzed until the peak point, 26% of the strain energy up to the failure corresponds to the intact-fibers phenomenon and the remaining 74% corresponds to fragmentation.

Table 2: Constituent properties of a typical CFRP composite (Swolfs et al. 2015)

Parameter	Value
Fiber volume fraction, V_f	0.40
Longitudinal fiber modulus, E_f	230 GPa
Characteristic strength, σ_0	5000 MPa
Characteristic length, L_0	25.0 mm
Weibull modulus, β	7.0
Interfacial shear stress, $\tau_{\text{Fiber/Epoxy}}$	50 MPa

2.4 Fiber-matrix interfacial strength, τ: Measurement uncertainty and influence on the σ vs ε curve

As mentioned before, models based on GLS approach overestimate the value of the ultimate tensile strength, $\sigma_{ultimate}$, in the composites. According to (Swolfs et al. 2015), this is probably caused because GLS neglects the stress concentrations when fiber breakage occurs and supposes that when a crack appears in any fiber, the load in the rupture

plane is uniformly transferred to the remaining intact fibers (Curtin 1991a). The global property that accounts for the load carrying from the matrix to the intact fibers, when a fiber rupture occurs, is the fiber-matrix interfacial strength, τ. There exist mainly three kinds of mechanical tests to determine that property: micro-bond test, pull-out test and tensile dog-bone test (Gaur and Miller 1989)(Zhandarov and Mäder 2014) (Feih et al. 2004), with obtained values of τ that can be significantly different each other for the same fiber-matrix interface. In the first type of tests, one drop of the matrix is fully held by the filament (Figure 3a), whereas in the second one, the drop is lying on a substrate (Figure 3b). Once the solidification of the matrix takes place, fiber is extracted and the force is measured, obtaining a Force vs. Displacement plot, as shown in Figure 4 for a typical pull-out test. Due to the small sample dimensions involved in the first two types of tests (micro-bond and pull-out), error sources are difficult to control and the repeatability and reproducibility of the experiments are low.

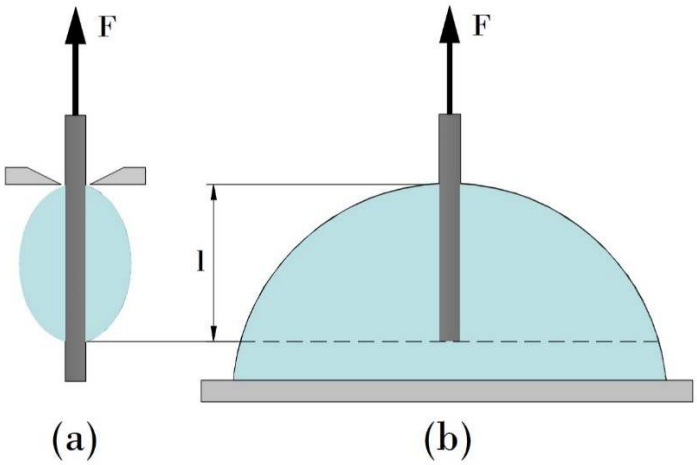

Figure 3: Mechanical test to determine the fiber-matrix interfacial strength, τ. a) Micro-bond test, b) Pull-out test.

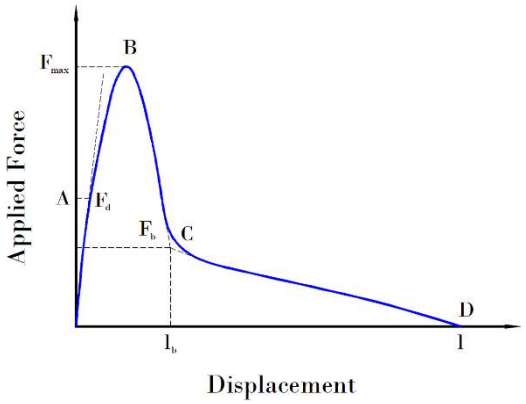

Figure 4: Typical Force vs. Displacement plot of a pull-out test (Zhandarov and Mäder 2014)**.**

On the other hand, in the tensile dog-bone test, a sample consisting on a single fiber embedded in a matrix is subjected to axial load and several fragments of fibers are formed as the deformation increases (Figure 5). In this test, the interfacial strength is estimated using the following equation:

$$\tau = \frac{\sigma_f \, d}{4 \cdot l_c} \tag{16}$$

Where σ_f is the tensile strength of the fiber, *d* is the fiber diameter and l_c is the critical length. To understand the concept of critical length, l_c, let us considered a single-fiber sample that is subjected to axial load. According to Oshawa et al. (Ohsawa et al. 1978), the tensile stress that is transferred to a fiber fragment by the matrix at a distance *x* from one edge of that fragment is given by:

$$\sigma_x = \frac{4\,\tau}{d} x \tag{17}$$

When the maximum stress reaches the tensile strength of the fiber, i.e., $\sigma_x = \sigma_f$, the corresponding distance in equation (17) is called x_0, in such a way that (Feih et al. 2004):

$$\sigma_f = \frac{4\,\tau}{d} x_0 \tag{18}$$

If the length of one fiber fragment is larger than $2x_0$, the rupture is still possible in that fragment, in such a way that when the length of all fragments is lower than $2x_0$, the fiber fragmentation is not possible anymore, the crack saturation is achieved and the ultimate tensile strength of the composite is obtained. According to (Feih et al. 2004), the average length of the fragments is given by:

$$\bar{l} = \frac{1}{2}(x_0 + 2x_0) = \frac{3}{2} x_0 \tag{19}$$

The critical length can be considered as $l_c = 2x_o$, and thereby the equation (19) can be rewritten as follows:

$$l_c = \frac{4}{3}\bar{l} \tag{20}$$

Accordingly, in the dog-bone tensile method, the average length of the fragments is measured, the critical length is computed using equation (20) and then the fiber-matrix interfacial strength is retrieved from equation (16). This method is valid only when the elastic modulus of the matrix is significantly lower than the one of the fiber. As this method implies the use of average quantities in one test, measures of statistical dispersion shall be taken into account in the calculations (variance, standard deviation, coefficient of variation, etc.). Both the measures of central tendency and dispersion can differ considerably from one experiment to another, which means that the repeatability and reproducibility of the dog-bone tensile method are low as well. Therefore, it can be concluded that the experimental measurement of the fiber-matrix interfacial strength, τ, can carry out an important uncertainty. This experimental inaccuracy in the determination of τ is one of the principal error sources of analytical and numerical models where this property is a fundamental input. For instance, Ferreira and Wang proposed a continuous modeling technique to simulate the fiber debonding and pull-out processes from a cement matrix using different interface mechanical properties. Interface elements with cohesive surface tractions were used in the fiber-matrix interface to simulate debonding process, whereas spring elements with a variable stiffness related to the shear stress were employed for the pull-out process (Friedrich and Wang 2016). According to the numerical results, a change from τ=1.5 MPa to τ=2.5 MPa, which is a possible deviation between experimental tests, considerably influences the behavior of the pull-out force with the slip displacement, leading, for example, to an increase of the maximum pull out force from 9.5 N to 15 N, approximately. Thereby, considering the uncertainty in the measurement of τ and its strong influence in the stress-strain behavior of the composite, this property can be taken as the adjustable micromechanical parameter in the present work.

The modification of the fiber-matrix interfacial strength could change the behavior of the GLS-based models. To show this, the effect of τ on the curve $\sigma\ vs\ \varepsilon$ of a CFRP material whose properties are listed in Table 3, is depicted in Figure 6. As can be observed, the decrease of τ allows 'contracting' the curve and 'relocating' the ultimate tensile strength, keeping constant the Young modulus of the material, namely, not altering the behavior of the material in the linear elastic zone, where the original models have demonstrated to be accurate enough.

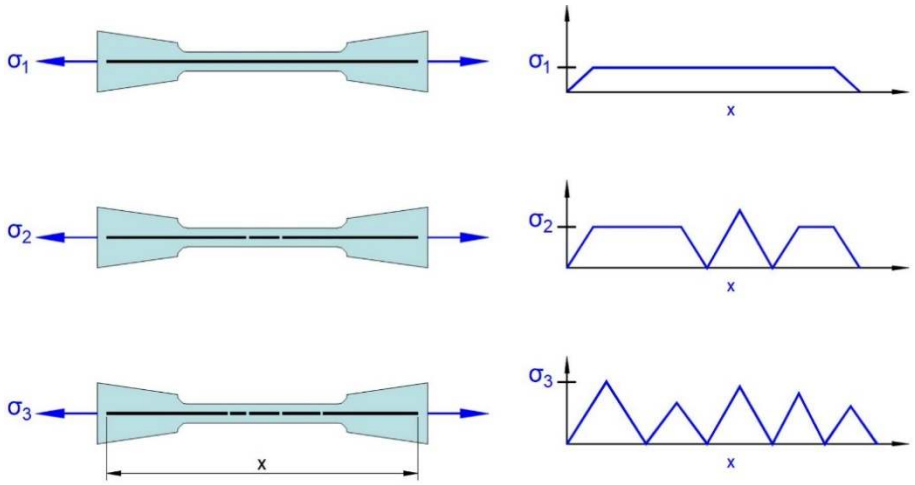

Figure 5: Scheme of fiber fragmentation of the single-fiber sample in the dog-bone tensile test. To the left, fiber fragmentation as the strain increases. To the right, stress on the fragments of fiber as a function of the position, where stress is zero at the positions corresponding to the broken fibers.

Table 3: Constituent properties, critical number of breaks and overall fragmentation limit stress of a T700SC/Epoxy composite.

Parameter	Value
Fiber volume fraction, V_f	**0.40**
Longitudinal fiber moduli, E_f	**220 GPa**
Fiber diameter, d	**7.0 µm**
Characteristic strength, σ_0	**5470 MPa**
Characteristic length, L_0	**20.0 mm**
Weibull modulus, β	**5.6**
Overall fragmentation limit stress, σ_c'	**13756.3 MPa**
Critical number of breaks, Λ_c	**269.4E-4 mm^{-1}**

2.5 Estimation of corrected fiber-matrix interfacial strength, τ^*.

In this point, it is important to highlight again that the CNB model is accurate enough to predict the tensile strength. Therefore, the fiber-matrix interfacial strength, τ, can be fitted in such a way that the ultimate tensile strength, $\sigma_{ultimate}$, is equal to the tensile strength calculated by the CNB model, σ_{CNB}. Consequently, an objective function can be defined as:

$$F = \sigma_{ultimate}(\tau) - \sigma_{CNB} \tag{21}$$

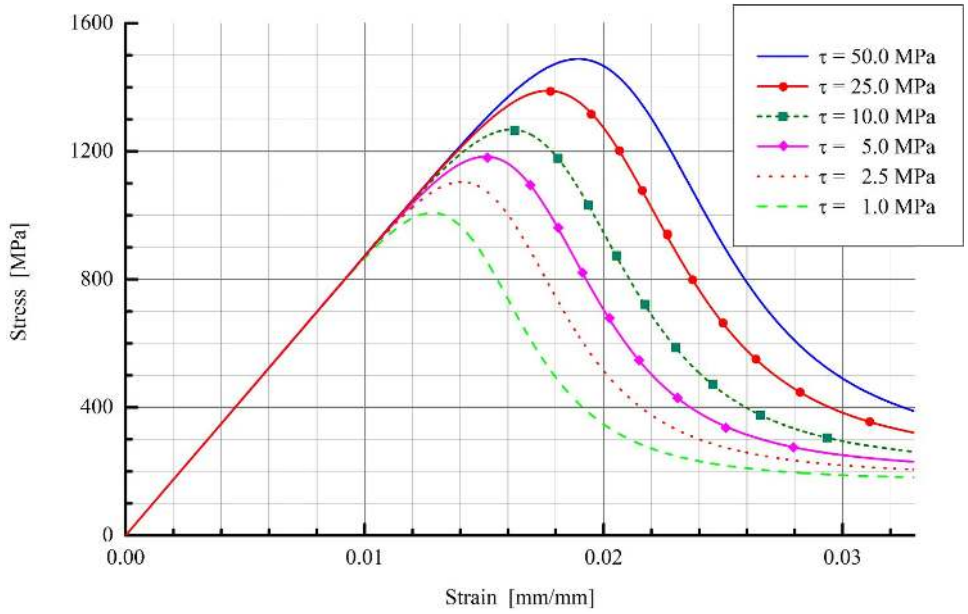

Figure 6: Influence of the fiber-matrix interfacial strength, τ, in the σ vs ε curve of a typical CFRP using the Neumeister model.

In this case, the goal is to find the value of τ for which $F \approx 0$. This value is called here the corrected fiber-matrix interfacial strength, τ^*, and it is estimated numerically using the Least Squares Method for non-linear equations in bounded domains. This method can be applied to solve the equation defined by $F = 0$ using the function *lsqnonlin* of MATLAB™. This function minimizes the sum of squares of the residuals, r_i, which in turn is given by $S = \sum_i (r_i)^2$, in a determined interval defined by τ_{min} and τ_{max}, with a guess given by τ_o. Considering that local minimums can be found under the stopping condition of *lsqnonlin*, which is the change of S relative to its initial value, and there is not any well-defined criterion here to establish a tolerance for such condition, it is necessary to define subintervals and minimize the sum of squares of the residuals, S, in each subinterval, modifying, recursively, the values of τ_o, τ_{min} and τ_{max}. The corrected fiber-matrix interfacial strength, τ^*, numerically computed, should fulfill the equation $|F| \leq \epsilon$, with ϵ as the prescribed error. The numerical code developed here to calculate an approximate value for τ^* is shown in Figure 7. As can be observed, the guess (τ_o), minimum value (τ_{min}) y maximum value (τ_{max}) of each cycle j are defined by:

$$\tau_o(j) = \tau(j-1) + \Delta\tau \tag{22}$$

$$\tau_{min}(j) = \tau_o(j) \tag{23}$$

$$\tau_{max} = 60 \times 10^6 \text{ Pa} \tag{24}$$

where $\tau(0) = 1 \times 10^5$ Pa, $\Delta\tau = 1 \times 10^{-6}$ and the error is considered as $\epsilon = 1 \times 10^{-3}$. The limits for the fiber-matrix interfacial strength, τ, used in the numerical code were established on the basis of the volumetric fiber content, V_f, of the composite. Thus, four typical CFRP and GFRP composites were considered (See Table 4), with V_f ranging between 0.15 and 0.40. For $V_f = 0.40$, the maximum value of the corrected fiber-matrix interfacial strength, τ^*, does not exceed $\tau^* = 60 \times 10^6 Pa$, whereas for $V_f = 0.15$, the minimum value is above $\tau^* = 1 \times 10^5 Pa$.

Table 4: Constituent properties, experimental tensile strength and overall fragmentation limit stress of several GFRP and CFRP composites systems

No.	1	2	3	4
Fiber	CARBON			GLASS
	T700SC	AS400	AS-4	
Matrix	Epoxi			
Ef (GPa)	230	294	234	76
d (μm)	6.9	7.1	7.1	13.0
σ_0 (MPa)	2700	4275	4275	1150

No.	1	2	3	4
Fiber	CARBON			GLASS
	T700SC	AS400	AS-4	
Matrix	Epoxi			
$L_0\ (mm)$	100.0	12.5	12.7	24.0
β	9.03	10.30	10.7	6.34
$\tau\ (MPa)$	23	40	40	42
Ref.	(Diao et al. 2014; Watanabe et al. 2014; Zhou et al. 2006)	(Matveev, Long, and Jones 2014)	(Curtin 2000)	(Okabe et al. 2001)
σ_C' (MPa)	12306.0	9871.9	8524.4	3956.3
σ_U (MPa)	1055	1890	1890	940

In order to calculate the ultimate tensile strength for a determined value of τ, $\sigma_{ultimate}(\tau)$, it is neccesary first to compute the ultimate strain of the composite, $\varepsilon_{ultimate}$, by solving the non-linear equation (12) using the Least Square Method too. However, in that case, it is not necessary to divide the principal interval into smaller subintervals since local minimums are not expected for the sum of squares of the residual, S, considering that in the curve $\sigma\ vs\ \varepsilon$ only a well-defined maximum point is present, which corresponds to the ultimate tensile strength of the composite (See Figure 6). Consequently, the solution of the non-linear equation (12) can be carried out in the interval for the strain defined by $\varepsilon_{min} = 0.005\ mm/mm$ and $\varepsilon_{max} = 0.03\ mm/mm$, with a guess given by $\varepsilon_o = 0.005\ mm/mm$. The inferior limit for the strain is taken as $\varepsilon_{min} = 0.005\ mm/mm$ because for lower values of ε, the CFRP and GFRP unidirectional composite materials of Table 4, when loaded along the fibers direction, are still in the elastic zone, as along as V_f ranges between 0.15 and 0.40. On the other hand, the superior limit for the strain is taken as $\varepsilon_{max} = 0.03\ mm/mm$ because for all composites considered here, the firsts two abovementioned phenomena (intact fibers in the elastic zone and fragmentation) have been fully developed for that level of strain. The schematic process to compute numerically the corrected fiber-matrix interfacial strength, τ^*, is depicted in Figure 7.

From now on, this new numerical model, which combines the capacity of a fitting model to predict the ultimate tensile strength of unidirectional composites (CNB model) (Vanegas-Jaramillo et al. 2018) with the recursive correction of a micromechanical parameter, τ, to change the behavior of the σ vs. ε curve without altering the stiffness of the material, will be referred as the $CNB + \tau^*$ model.

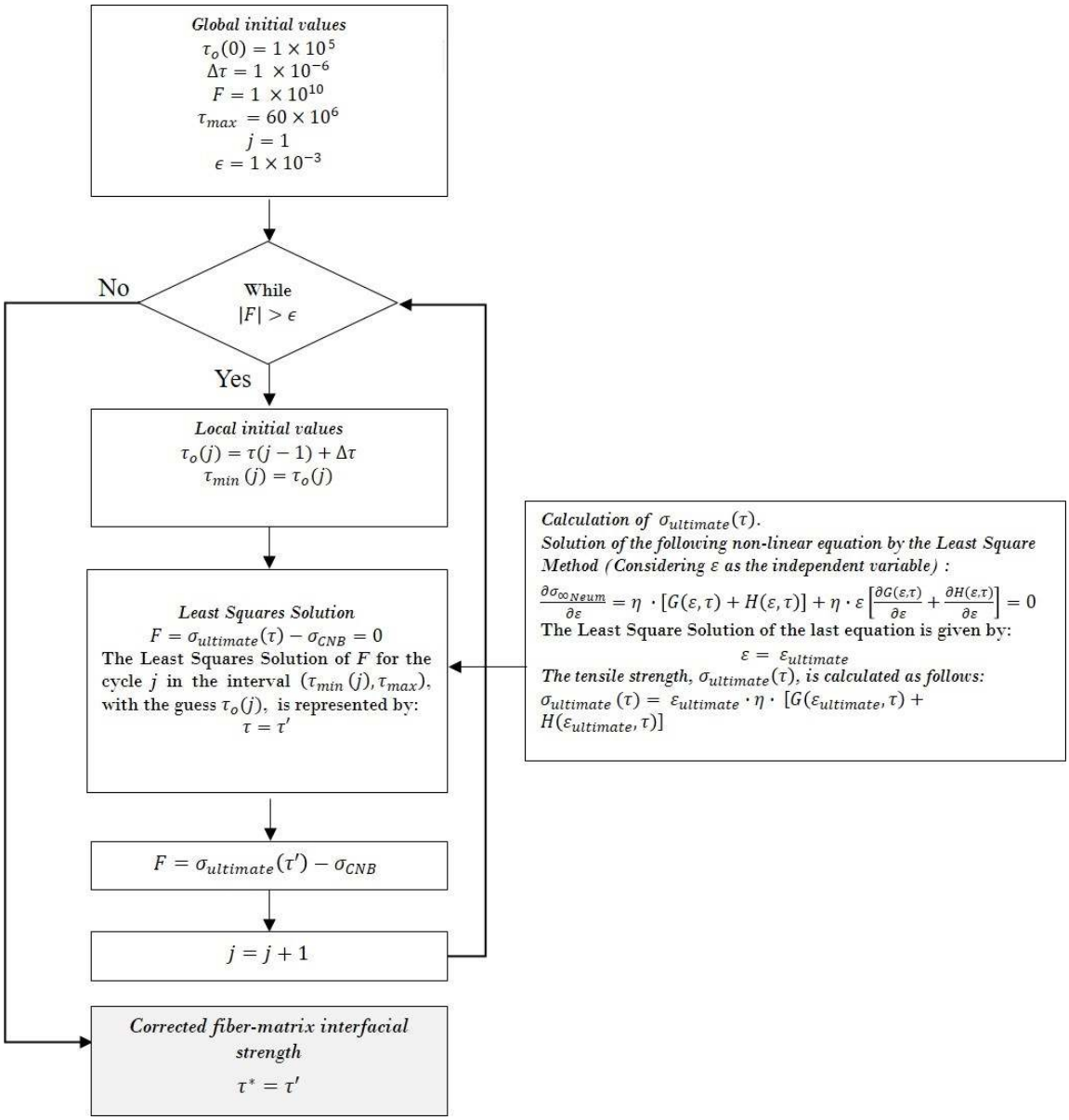

Figure 7: Numerical code to compute the corrected fiber-matrix interfacial strength, τ*.

3 RESULTS AND DISCUSSIONS.

3.1 Assessment of the $CNB + \tau^*$ model.

In Table 4, the constituent properties, experimental tensile strength and overall fragmentation limit stress of several GFRP and CFRP composites are reported. The $CNB + \tau^*$ model developed in the present work is used to predict the stress-strain behavior of the material 1 shown in that table, which corresponds to carbon fibers T700SC reinforced with an epoxy matrix. The corrected fiber-matrix interfacial strength computed by the numerical code of Figure 7 is $\tau^* = 1.78\ MPa$, which is much lower than the value reported in Table 4, $\tau = 23\ MPa$. This happens because the CNB+τ* is essentially a fitting model that 'contracts' the original σ vs. ε curve predicted by the Neumeister equation, taking into account the ultimate tensile strength obtained by CNB (which is in turn a model that considers the experimental values of $\sigma_{ultimate}$) and modifying, recursively, the fiber-matrix interfacial strength, τ*. Accordingly, there are several effects present in a real test that are implicit in the $CNB + \tau^*$ model, but are not considered in the original Neumeister model, which is purely analytical; for instance, the influence of the stress concentration around the broken fibers on the stress distribution and the effect of the fiber packing on the load transferring from the matrix to the fibers. In this work, the micromechanical parameter τ is fitted to account for these effects implicitly and obtain a more realistic stress-strain response of the composite.

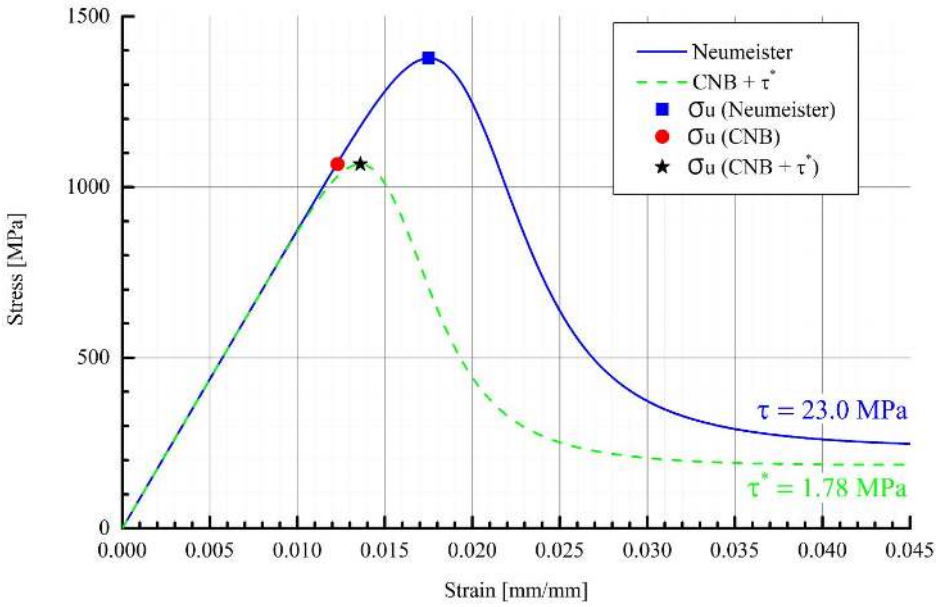

Figure 8: Comparison of σ vs. ε curves of the composite CFRP T700SC/EP obtained by original Neumeister and CNB+τ*

According to the original Neumeister model, equation (1), for a fiber volume content of $V_f = 0.38$, the ultimate tensile strength and ultimate strain of material 1 of Table 4 are $\sigma_{U,Neum} = 1377.40\ MPa$ and $\varepsilon_{U,Neum} = 1.75 \times 10^{-2}$, respectively (See blue square marker in Figure 8). The ultimate tensile strength predicted by the Neumeister model, $\sigma_{U,Neum}$, considerably exceeds the experimental one reported in Table 4, $\sigma_{U,exp} = 1055\ MPa$, obtaining a relative difference of *d=30.55%,* where $d = \left|\sigma_{U,exp} - \sigma_{U,teo}\right| / \sigma_{U,exp}$ and the theoretical strength in this case is $\sigma_{U,teo} = \sigma_{U,Neum}$. On the other hand, if the $CNB + \tau^*$ model described in Section 2 is used to correct the σ vs. ε curve of the composite, the dashed green line of Figure 8 is obtained. Let us remember that the $CNB + \tau^*$ model comprises two principal steps: 1) the calculation of the ultimate tensile strength by the CNB model (Vanegas-Jaramillo et al. 2018), σ_{CNB}, which is represented in the original Neumeister curve of Figure 8 by a red dotted marker, 2) the 'contraction' of the Neumeister curve by means of the corrected fiber-matrix interfacial strength, τ^*, to obtain a peak point corresponding to σ_{CNB} (see black, star-type marker). In this case, the ultimate tensile strength and strain predicted by $CNB + \tau^*$ are $\sigma_{U,teo} = \sigma_{U,CNB+\tau^*} = 1067.3\ MPa$ and $\varepsilon_{U,CNB+\tau^*} = 1.36 \times 10^{-2}$, respectively. The relative difference with the experimental result of Table 4 is *d=1.16%*, which is significantly lower than the one obtained with the original Neumeister model. This satisfactory result is obtained because CNB is a reliable fitting model to estimate the ultimate tensile strength of GFRP and CFRP composites, as it was demonstrated in (Vanegas-Jaramillo et al. 2018), and additionally, the correction of the fiber-matrix interfacial strength using the numerical code shown in Figure 7, allows relocating the maximum point of the σ vs. ε curve, without altering the Young modulus of the material.

In this point, it is important to remember an important premise of the fiber fragmentation models: the ultimate tensile strength should correspond to the critical density of fiber breaks, Λ_C, where the crack saturation is reached. In Figure 9, the σ vs. Λ curves predicted by Neumeister and CNB+τ* models are compared. These curves can be obtained considering that the density of fiber breaks, Λ, is related to the fiber stress, σ_f, and damage variable, w, by the following equations (Vanegas-Jaramillo et al. 2018):

$$\sigma_f = (\Lambda\, L_0)^{\frac{1}{\beta}} \cdot \sigma_0 \tag{25}$$

$$w = 2L_c \cdot \Lambda \tag{26}$$

As can be observed in Figure 9, the critical density of fiber breaks, Λ_C, predicted by the Neumeister model is $\Lambda_{c,Neum} = 3.35 \times 10^{-2}\ mm^{-1}$ (blue square marker), whereas the one predicted by the $CNB + \tau^*$ model is $\Lambda_{c,CNB+\tau^*} = 3.47 \times 10^{-1}\ mm^{-1}$ (black, start-type marker). In general, the values of Λ_C predicted by our $CNB + \tau^*$ model for all materials reported in Table 4 are larger than the values predicted by the Neumeister model. This happens because, as mentioned before, the corrected interfacial strength, τ^*, computed here is lower than the interfacial strength obtained experimentally, τ, and according to previous results (Vanegas-Jaramillo et al. 2018), the reduction of the fiber-matrix interfacial strength, τ, leads to the decrease of the average length of the fiber fragments (which is equivalent to the increase of Λ).

Some energetic contributions in the stress-strain curve of the material CFRP T700SC/EP until the failure are represented in Figure 10. Two zones can be clearly differentiated: zone of intact fibers (green zone) and zone of fragmentation (orange zone). The zone of separation/sliding is not considered since it is not relevant for this particular analysis. According to experimental works in unidirectional carbon/epoxy composites (Rochardjo et al. 1997), for the levels of fiber volume content considered here, the composite fracture is dominated by the phenomena arising in the intact fibers and fragmentation zones, whereas for high fiber volume fractions, fiber pull out needs to be considered. In the first zone (green), cracks are not present and the mechanical response of the material is linear elastic (Hooke's law). In the second zone (orange), the fiber fragmentation occurs until the crack saturation is reached and the composites fails. The internal strain energy per unit volume released during the damage process is $U_T = 7.91\ MJ/m^3$, from which 21.3% corresponds to the zone of intact fibers and the remaining 78.7%, to the zone of fragmentation.

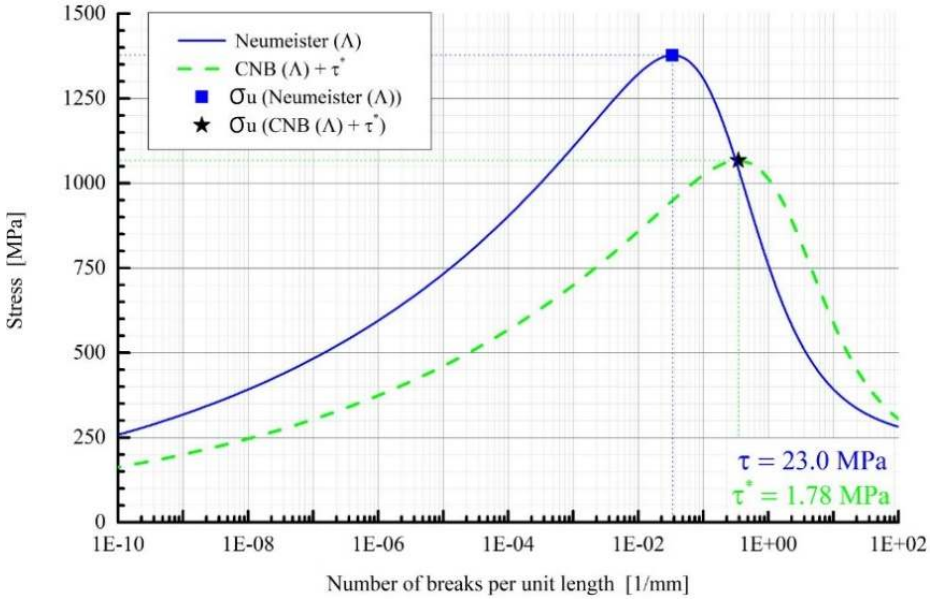

Figure 9: Comparison of σ vs. Λ curves of the composite CFRP T700SC/EP obtained by original Neumeister and $CNB + \tau^*$

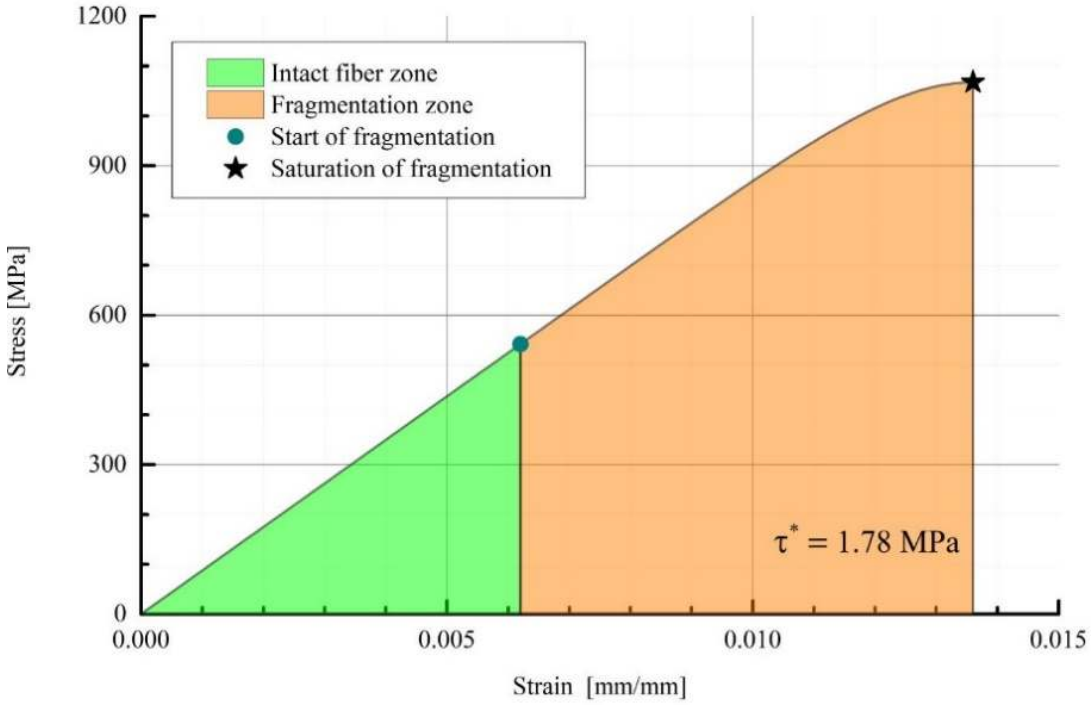

Figure 10: Energetic contributions in the σ vs. ε curve of the material CFRP T700SC/EP predicted by CNB+τ*, until the failure point.

It is important to remember that CNB+τ* is a semi-empirical model that makes use of several experimental data to predict the tensile response of unidirectional CFRP and GFRP composites. These data were previously presented in (Vanegas-Jaramillo et al. 2018) and are summarized in Table 5 in the present work. In that table additional experiments are considered to validate the present model. In total, 25 experiments were searched in the scientific literature, obtaining a maximum and average relative difference of d_{max}=15.67% and d_{ave}=5.01%, respectively, which allows concluding that the present model predicts acceptable results when compared to experiments. As reasonable, the relative differences are smaller for the experiments that were directly considered in the deduction of the present model, however, for the additional experiments that were examined in the present work, not directly deemed in the model deduction, acceptable differences were obtained. For instance, let us consider the results of a recent benchmarking of strength models for unidirectional composites under longitudinal tension (Bunsell et al. 2018), whose experimental parameters are reported in row 22 of the Table 5. In that work, four different model approaches were evaluated: hierarchical scaling law, direct numerical simulation with linear-elastic matrix, direct numerical simulations with elastic-perfectly-plastic matrix and multiscale FE^2 model. The relative difference between the present CNB+τ* model and the experiment of that benchmarking exercise is 11.05%. For the four models assessed in the benchmarking (Bunsell et al. 2018), this difference is approximately: 2.16% for hierarchical scaling law, 82.41% for direct numerical simulation with linear elastic matrix, 59.61% for direct numerical simulations with elastic-perfectly-plastic matrix and 18.59% for multiscale FE^2 model. Thereby, the present model predicts more accurate results than the last three mentioned models. The graphical comparison among all models and experimental results is shown in Figure 11.

Table 5: Comparison between the tensile strengths predicted by CNB+τ* and obtained in several experimental works.

	Composites information and properties										Calculations and assessment of the proposed model			
	Sources	Composite system	Fiber volume content, V_f	Young Modulus of fiber, E_f (Gpa)	Fiber diameter, d (μm)	Characteristic stress, σ_o (Mpa)	Characteristic length, L_o (mm)	Weibull modulus, β	Fiber-matrix interfacial shear strength, τ (Mpa)	Experimental tensile strength, σu (Mpa)	Overall fragmentation limit stress, σ_c' (Mpa)	Critical number of breaks density, Λ_c (1/mm)	σu, CNB+τ* (MPa)	*Relative difference (%)*
Experiments considered in this semi-empirical model	(Diao et al. 2014) (Zhou et al. 2006) (Watanabe et al. 2014)	T700SC/ Epoxy	0.38	230	6.9	2700	100	9.03	23	1055	12306	1.47E-02	1067	*1.18*
	(Matveev et al. 2014)	AS400/ Epoxy	0.59	294	7.1	4275	12.5	10.3	40	1890	9872	3.06E-03	1836	*2.84*
	(Matveev et al. 2014)	T700 / Epoxy	0.70	220	7.0	5470	20	5.6	40	3409	13756	3.13E-02	3497	*2.59*
	(Koyanagi et al. 2009)	M40/ Epoxy	0.59	392	6.0	4500	25	16	50	2310	9955	3.24E-03	2268	*1.80*
	(Curtin 2000)	AS4/ Epoxy	0.68	234	7.1	4275	12.7	10.7	40	1890	8524	1.09E-03	1939	*2.61*
	(Curtin 2000)	AS4/ Epoxy	0.68	234	7.1	4493	10	8.33	40	1890	9374	2.11E-03	1914	*1.27*
	(Koyanagi et al. 2009)	M40/ Vinilester	0.30	392	6.0	4500	25	16	20	1390	18551	1.45E-01	1390	*0.03*
	(Okabe et al. 2001)	E-glass/ Epoxy	0.57	76	13.0	1150	24	6.34	42	940	3956	1.03E+00	940	*0.00*
	(Diao et al. 2014)	E-glass/ Epoxy	0.38	72	14.9	1649	5	3.09	23	719	7537	5.13E-01	715	*0.61*
	(Koyanagi et al. 2009)	E-glass/ Vinilester	0.10	72	16.0	2500	25	13	40	252	32732	5.29E-02	255	*1.01*

	Composites information and properties										Calculations and assessment of the proposed model			
	Sources	Composite system	Fiber volume content, V_f	Young Modulus of fiber, E_f (Gpa)	Fiber diameter, d (μm)	Characteristic stress, σ_o (Mpa)	Characteristic length, L_o (mm)	Weibull modulus, β	Fiber-matrix interfacial shear strength, τ (Mpa)	Experimental tensile strength, σu (Mpa)	Overall fragmentation limit stress, σ_c' (Mpa)	Critical number of breaks density, Λ_c (1/mm)	σu, CNB+τ* (MPa)	*Relative difference (%)*
Additional experiments	(Beyerlein and Phoenix 1996a; DeMorais 2006)	Carbon AS4/ Epoxy 934	0.54	230	7.0	4040	10	11	48	1586	10034	3.43E-03	1605	*1.21*
	(Beyerlein and Phoenix 1996a; DeMorais 2006)	Carbon AS4/ Epoxy 934	0.60	230	7.0	4493	10	5	48	1792	13234	2.42E-02	2024	*12.94*
	(Beyerlein and Phoenix 1996a; DeMorais 2006)	Carbon AS4/ Epoxy 937	0.57	230	7.0	4493	10	5	52	1930	14120	3.70E-02	2090	*8.28*
	(Beyerlein and Phoenix 1996a; DeMorais 2006)	Carbon AS4/ Epoxy937	0.63	230	7.0	4493	10	5	52	2206	12775	1.90E-02	2027	*8.09*
	(Beyerlein and Phoenix 1996a; DeMorais 2006)	Carbon AS4/ Epoxy 8551.7	0.63	234	7.0	4493	10	5	56	2170	12936	2.07E-02	2062	*4.97*
	(Beyerlein and Phoenix 1996a; DeMorais 2006)	Carbon AS4/ Epoxi APC-2	0.58	234	7.0	4493	10	5	58	2060	14123	3.71E-02	2128	*3.29*
	(Beyerlein and Phoenix 1996a; DeMorais 2006)	Carbon AS4/ Epoxy APC-2	0.66	234	7.0	4493	10	5	58	2297	12411	1.56E-02	2042	*11.11*
	(DeMorais 2006; Fukuda and Miyazawa 1994)	Carbon T300/ Epoxi 934	0.60	232	7.1	3170	30	5.1	48	1790	11701	1.03E-02	1509	*15.67*
	(DeMorais 2006; Fukuda and Miyazawa 1994)	Carbon T300/ Epoxy 914	0.60	232	7.1	3170	30	5.1	28	1432	10696	5.43E-03	1331	*7.03*
	(DeMorais 2006; Fukuda and Miyazawa 1994)	Carbon T300/ Epoxy 3631	0.57	232	7.1	3170	30	5.1	52	1760	12481	1.62E-02	1566	*11.00*
	(Na et al. 2017)	Carbon T700/ Bisphenol A type Epoxy Epofix	0.55	217	7.0	3927	10	12.0	37	1506	9196	1.85E-03	1549	*2.84*
	(Bunsell et al. 2018)	Carbon T800/ EpoxiyM21	0.55	294	5.0	3900	100	4.8	96	3070	23269	1.56E-01	3409	*11.05*
	(Curtin and Takeda 1998b; Madhukar and Drzal 1991)	Carbon AS4C/ Epoxy 828eponmPDA	0.68	241	7.1	4298	12.7	10.7	45	2044	8622	1.18E-03	1973	*3.48*
	(Chang et al. 1994; Curtin and Takeda 1998b)	Carbon AS4/ Thermoplastic J2	0.58	234	7.0	4275	12.7	10.7	40	1830	9971	3.28E-03	1842	*0.63*
	(Chang et al. 1994; Curtin and Takeda 1998b)	Carbon AS4C/ Thermoplastic J2	0.54	241	7.1	4275	12.7	10.7	41	1640	10709	5.48E-03	1798	*9.63*
						AVERAGE RELATIVE DIFFERENCE								*5.01*
						MAXIMUM RELATIVE DIFFERENCE								*15.67*

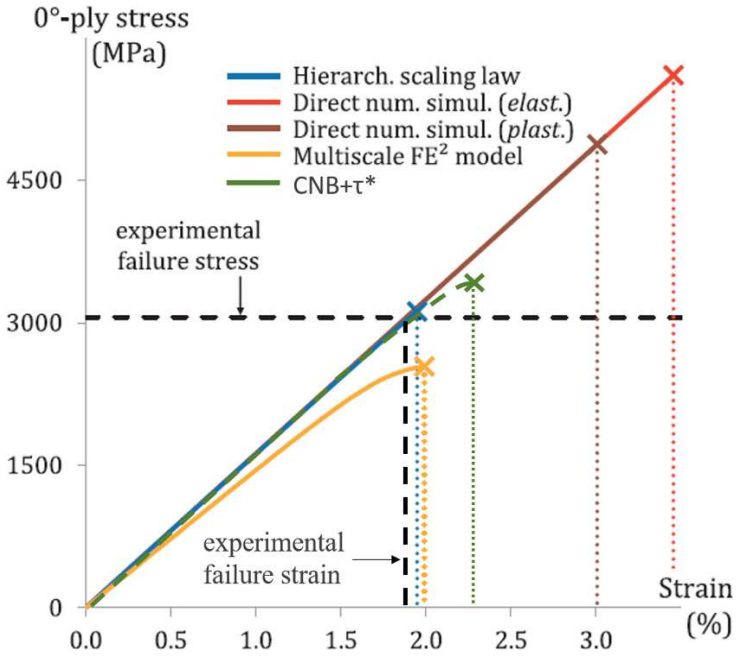

Figure 11: Stress vs. strain curves obtained by several models and comparison with experimental results. This figure was redrawn from (Bunsell et al. 2018)

3.2 Influence of the fiber volume content on the mechanical response predicted by $CNB + \tau^*$ model.

In Figure 12, it is shown the influence of the fiber volume content, V_f, on the mechanical response of the T700SC/EP composite analyzed in Section 3.1. In that figure, two phenomena arising during the damage process of the composite are identified as IF (Intact fibers) and FM (Fragmentation). As expected, $CNB + \tau^*$ model predicts that the higher the fiber volume content, V_f, the larger the ultimate tensile strength, $\sigma_{ultimate}$, and the Young modulus of the composite, E. However, $CNB + \tau^*$ model does not predict a monotonic behavior of the ultimate strain, ε_u, with the fiber volume content, V_f, and this can be explained considering two effects: 1) the reduction of the strain with V_f in the elastic zone for a given stress, and 2) the influence of V_f on the development of the fiber fragmentation phenomenon. In the first case, for a given stress lying in the elastic zone of all materials, the higher V_f, the lower the corresponding strain, which is reasonable considering the increase of the Young modulus, E, with V_f.

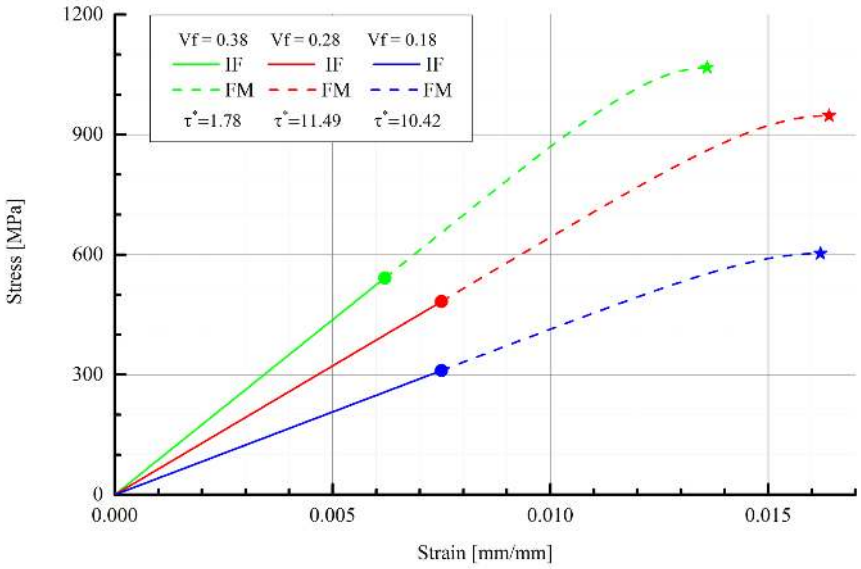

Figure 12: Influence of the fiber volume content, V_f, on the stress-strain response of the material CFRP T700SC/EP predicted by CNB+τ*.

On the other hand, in the second case, the effect of V_f on the fiber fragmentation zone, which is delimited between the dotted and the star-type markers in each σ vs. ε curve of Figure 12, is not monotonous. For instance, if the σ vs. ε curves for $V_f = 0.38$ *(green curve)* and $V_f = 0.28$ *(red curve)* are compared each other, it can be noticed that the reduction of the fiber content, V_f, brings about an important increase of the strain corresponding to the start of fragmentation (dotted markers) and, additionally, to the broadening of the fragmentation zone, which in turns leads to the increase of the ultimate strain, from $\varepsilon_u = 1.36 \times 10^{-2}$ for $V_f = 0.38$ to $\varepsilon_u = 1.64 \times 10^{-2}$ for $V_f = 0.28$. However, if the σ vs. ε curves for $V_f = 0.28$ *(red curve)* and $V_f = 0.18$ *(blue curve)* are compared each other, it can be noticed that the both the strain corresponding to the start of fragmentation and the ultimate strain slightly decreases with the reduction of the fiber content, V_f, with $\varepsilon_u = 1.62 \times 10^{-2}$ for $V_f = 0.18$. A possible explanation for this can be addressed considering two phenomena: 1) the stress concentration around fiber breaks and 2) the damage progression in a transverse plane. In general, the stress concentration around the fiber breaks is lower as the fibers are farther each other, namely, as the fiber volume content, V_f, is lower, leading to a higher ultimate strain, ε_u, since the stress distribution is more uniform. This phenomenon seems to be predominant from $V_f = 0.38$ to $V_f = 0.28$. On the other hand, the damage progression in a transverse plane of the composite strongly depends on the fiber volume content, V_f. As the fibers are farther each other, namely, as V_f is lower, the probability to obtain a determined number of fiber breaks in a transverse plane increases, which means an increase of the damage probability of the composite before reaching a determined deformation. This phenomenon seems to be predominant from $V_f = 0.28$ to $V_f = 0.18$. The increase of the fragmentation strain with the fiber volume content was reported in the experimental work of (Mazen, Metwalli, and El-Mahallawy 2007), where the influence of four different fiber volume fractions (9.2%, 18.4%, 27.6% and 36.8%) on the tensile deformation behavior of epoxy-matrix composites reinforced with glass, carbon and hybrid fibers was studied; in those particular experimental tests, the second abovementioned phenomenon seems to be predominant.

Now, let us consider the influence of the fiber volume content, V_f, on the energetic contributions of the two phenomena analyzed here (IF and FM) for the curves represented in Figure 12. In Table 6, the internal strain energy per unit volume for the IF and FM zones of each curve are reported. Several aspects are worth-mentioning according to the results obtained. Firstly, according to our model, the total strain energy does not increase monotonically with V_f, since the biggest energy released until the failure point was obtained for the intermediate fiber volume content, $V_f = 0.28$, where $U_T = 8.48\ MJ/m^3$. This happens because the increase of V_f has a two opposite effects on the fracture toughness of the composite material: the higher V_f, the larger the Young modulus and the ultimate tensile strength, which contributes to the fracture toughness; however, the higher V_f, the larger the number of filaments per unit volume, and consequently, the stress concentration around the fiber breaks, which has an adverse effect on the fracture toughness.

Another aspect that can be noticed is that the percent energetic contribution of the IF and FM zones to the total strain energy is very similar for all fiber volume contents considered here, with an average of 21.49% for the IF zone and 78.51% for the FM zone. This means that the relationship between the strain energy released due to the composite elongation in the linear elastic zone (IF) and the strain energy released due to the fiber fragmentation process (FM) does not change considerably with V_f for this particular case. Considering a parameter defined by $r_{FM/IF} = \left[\sum_{j=1}^{n}(E_{FM}/E_{IF})_j\right]/n$, where $(E_{FM}/E_{IF})_j$ is the ratio of the energy released in the fragmentation zone to the energy released in the elastic zone for the fiber volume content defined by "*j*", and "*n*" is the number of fiber volume contents considered, this parameter is $r_{FM/IF} = 3.66$ in this case. This means that the strain energy released in the FM zone is approximately 3.66 times larger than the strain energy released in the IF zone.

Table 6: Influence of the fiber volume content, V_f, on the internal strain energy per unit volume considering IF and FM zones.

Fiber volume content, V_f	Corrected Tau, τ^* MPa	Internal strain energy per unit volume				
		Total	Intact fibers (IF)		Fragmentation (FM)	
		MJ/m³	MJ/m³	%	MJ/m³	%
0.18	10.42	5.32	1.16	21.88	4.16	78.12
0.28	11.49	8.48	1.81	21.36	6.67	78.64
0.38	1.78	7.91	1.68	21.23	6.23	78.77

3.3 Stress-strain response of several composite systems using the $CNB + \tau^*$ model

The $CNB + \tau^*$ model offer the ability to obtain the ultimate strength, ultimate strain and total strain energy in terms of the constituent properties and the fiber volume content. So, using this model for each composite in a range of V_f, it is possible to predict the mechanical response in several scenarios of design. Accordingly, using $CNB + \tau^*$ model,

it is possible to develop novel mechanical-performance maps that allow finding the desirable mechanical performance of a composite or comparing quickly some composites to fulfill a particular requirement, i.e, a maximum tensile stress, an allowable deformation or a target toughness. The maps for the materials listed in Table 4 are shown in Figure 13 and Figure 14.

In this section, the $CNB + \tau^*$ model is used to study the tensile mechanical behaviour of the four composite systems reported in Table 4 using the mechanical-performance maps. For each material, a two y-axes plot showing the influence of the fiber volume content, V_f, on the total energy of the damage process, U_T (left y-axis) and on the corrected fiber-matrix interfacial strength, τ^* (right y-axis), is reported in Figure 13. In that figure, the total energy is disaggregated into the linear elastic energy (IF contribution, purple zone) and fragmentation energy (FM contribution, cyan zone). According to the plots, the behavior of U_T and τ^* with V_f is very different for GFRP and CFRP composites. For the CFRP composites, a non-linear behavior of U_T can be appreciated (Figures 13 a,b,c), whereas for the GFRP, a linear behavior is observed instead (Figure 13d). Additionally, for the CFRP composites, the maximum value of U_T is not reached in the maximum value of the fiber volume content considered here, $V_f = 0.4$, conversely to the case of the GFRP composites where U_T increases monotonically linear with V_f. Let us remember that the change of U_T with V_f was attributed to two opposite effects: the increase of the Young modulus and ultimate tensile strength with V_f, which increases the fracture toughness, and the increase of the stress concentration factor around the fiber breaks with V_f, which has an adverse effect on the fracture toughness. Therefore, according to the results, the first effect is predominant for the GFRP composite in this case. The material with the largest fracture toughness is AS-4/Epoxi composite with $V_f = 0.37$, where $U_T = 16.19\ MJ/m^3$.

As presented in Section 3.2, the $CNB + \tau^*$ model predicts that for the composite T700SC, the ratio of the energy released in the fragmentation zone to the energy released in the elastic zone is practically independent on the fiber volume content, V_f. If the previously defined parameter $r_{FM/IF}$ is computed again for this material and the remaining materials of Table 4, considering the range for V_f presented in Figure 13 (from $V_f = 0.15$ to $V_f = 0.4$), with V_f increasing by 0.1, results shown in Table 7 are obtained. Let us remember that $r_{FM/IF}$ is the average of the ratio between the fragmentation and elastic energies. In Table 7, the averages of the total, elastic and fragmentation strain energies ($\overline{U_{TOTAL}}$, $\overline{U_{IF}}$ and $\overline{U_{FM}}$), as well as the standard deviation of the ratio $r_{FM/IF}$, represented by $SD_{FM/IF}$, are reported for each composite. According to the relatively small values of $SD_{FM/IF}$, the previous result is confirmed: the ratio $r_{FM/IF}$ is almost independent on the fiber volume content, V_f. The largest value of $r_{FM/IF}$ is obtained for the GFRP composite, where the strain energy released in the FM zone is approximately 7.87 times larger than the strain energy released in the IF zone.

Table 7: Relationship between the energies released in the elastic and fragmentation zones for the CFRP and GFRP composites.

Composite	Average Internal strain energy per unit volume			$r_{FM/IF}$	$SD_{FM/IF}$
	$\overline{U_{TOTAL}}$	$\overline{U_{IF}}$	$\overline{U_{FM}}$		
	MJ/m³	MJ/m³	MJ/m³		
T700SC/EP	7.29	1.57	5.71	**3.63**	0.038
AS400/EP	9.44	2.47	6.97	**2.82**	0.027
AS-4/EP	11.81	3.27	8.54	**2.61**	0.020
Glass/EP	5.91	0.67	5.24	**7.87**	0.067

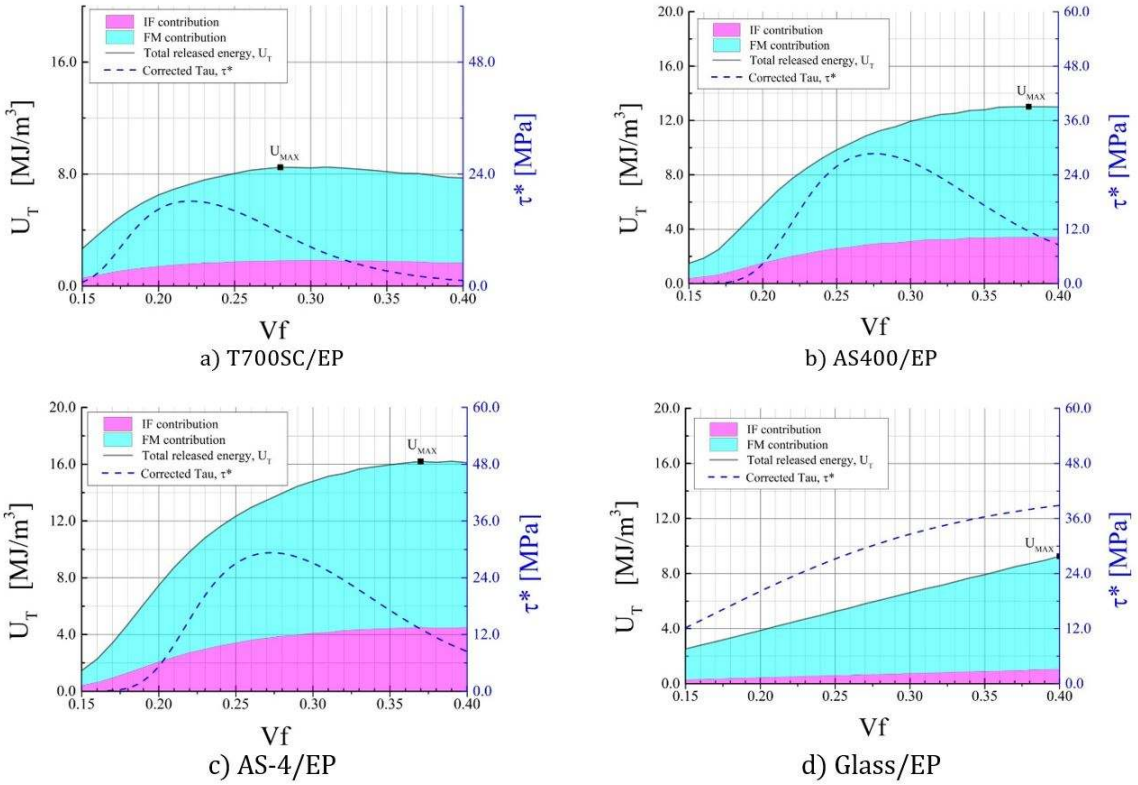

Figure 13: Mechanical-performance-maps with the influence of the fiber volume content, V_f, on both the released energy, $U_{(\text{Total, IF \& FM})}$, and the corrected fiber-matrix interfacial strength, τ^*, predicted by CNB+τ*.

Regarding the corrected fiber-matrix interfacial strength, τ^*, a similar conclusion can be addressed: it changes monotonically with V_f for the GFRP composite, whereas for the CFRP composites, a maximum point is obtained in between the minimum and maximum fiber content.

The mechanical-performance maps on Figure 14 are two y-axes plots where the change of the ultimate tensile strength, σ_u (left y-axis) and of the ultimate strain, ε_u (right y-axis) with V_f, for each one of the materials listed in Table 4, is shown. The $CNB + \tau^*$ model predicts a non-linear increase of the ultimate tensile strength, σ_U, with the fiber content, V_f, for the CFRP composites, whereas for the GFRP composite, this increase is linear. Theoretically, the ultimate tensile strength, σ_U, should increase with the fiber content, V_f, however, in some experimental works, the reduction of σ_U with V_f has been reported from a determined value of fiber content, and this can be attributed mainly to the manufacturing process. For instance, the decrease of σ_U with V_f for glass fiber/polypropylene composites, from $V_f = 20\%$ onwards, was reported in (Lee and Jang 1999), and such reduction was attributed to the void content of the composite, which was manufactured by a vacuum-assisted process. For carbon reinforced PTFE composites, a non-linear increase of σ_U with V_f until $V_f = 30\%$ was obtained in the experimental work of (Li 2010), in agreeing with the results obtained here for CFRP composites; however, from $V_f = 30\%$ onwards, the reduction of σ_U with V_f was reported; injection molding process was used in that work to manufacture the samples for the mechanical tests. A non-monotonic behavior of σ_U with V_f has been obtained as well for carbon-fabric/polycarbonate laminates prepared by a two-Step hot-press technique (Liu et al. 2018), unidirectional carbon/epoxy composite used in the design of an automobile suspension system (Ali and Anjaneyulu 2018), carbon fabric reinforced polyetherimide composites fabricated by impregnation techniques (Bijwe and Rattan 2007), among others; in all cases, in the zone where σ_u and V_f are directly proportional, the increase of σ_U with V_f is non-linear, coinciding with the present results of CFRP composites; additionally, the inflection point where the behavior of σ_U with V_f is modified mainly depends on the processing conditions of the composite. This processing conditions can entail many defects that affect the mechanical performance of the composite (Vanegas-jaramillo, Patiño-Arcila, and Vargas-Isaza 2013) and are not directly considered in many theoretical models.

For the ultimate strain, ε_u, a different behavior between the GFRP and CFRP composites is predicted as well: a non-monotonous variation of ε_u with V_f is obtained for CFRP, while for GFRP, an increasing change can be appreciated. On the basis of these results, another important difference between the GFRP and CFRP composites can be identified: in the first ones, the increase of σ_u entails an increase of ε_u, which does not happen for the second ones. The more resistant

material is AS-4 with $V_f = 0.4$, where $\sigma_u = 1601.5MPa$. On the other hand, the more ductile material is the glass composite with $V_f = 0.4$, where $\varepsilon_u = 0.0251mm/mm$. The behavior of ε_u with V_f in GFRP and CFRP composites has been experimentally studied too. In agreement with the present results, the tensile curves reported in (Yu et al. 2019) for additively manufactured continuous carbon fiber-reinforced polymer composites clearly shows that the ultimate tensile strain, ε_u, does not have a uniform behavior with the fiber content, whereas σ_U has an incremental behavior with V_f that is consistent with the results obtained here. Similar tendencies were obtained by (Naranjo-Lozada et al. 2019) for continuous fiber composites in a nylon matrix produced by additive manufacturing. On the other hand, another experimental works have obtained a different behavior of ε_u with V_f. For instance, the continuous decrease of ε_u with V_f was reported by (Yang et al. 2017) for carbon-fabric/polycarbonate composites, with V_f ranging between 18.6% and 35.2%, whereas an opposite behavior was reported for glass-fiber/epoxy composites with V_f ranging between 9.2% and 36.8%, namely, ε_u continuously increases with V_f (Mazen et al. 2007). In general, the former tendency, i.e, the reduction of ε_u with V_f, is observed in the CFRP composites using the present model in ranges that are relatively close to the one considered by (Yang et al. 2017); moreover, the second tendency, i.e., the increase of ε_u with V_f, also coincides with the one obtained here for GFRP composites; however, it is important to mention that the fiber configurations of these two experimental works is different to the unidirectional configuration considered here, and further experiments are needed to confirm the present numerical results.

In Table 8, the ultimate tensile strengths computed by the $CNB + \tau^*$ model and two additional analytical models, namely, Neumeister (Neumeister 1993a) and SFF (Koyanagi et al. 2009), for the composite systems reported in Table 4, are compared with experimental values. The ultimate tensile strengths computed by the $CNB + \tau^*$ model fit better to the experimental values than the ones computed by the other analytical models. For instance, considering the four composite systems listed in Table 8, the L^2 relative error norm of the $CNB + \tau^*$ model is 2.45%, whereas this value is 34.06% for Neumeister and 27.52% for SFF.

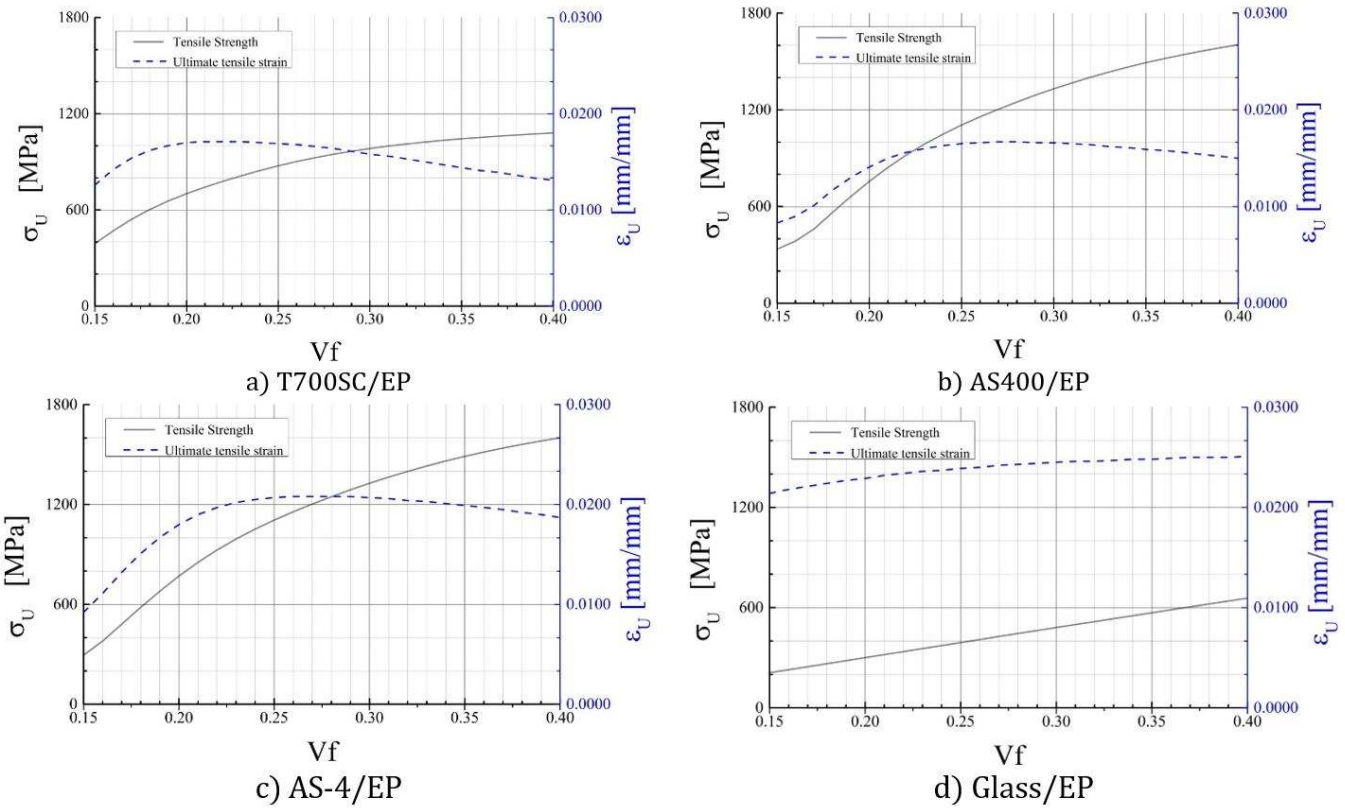

Figure 14: Mechanical-performance-maps with the influence of the fiber volume content, V_f, on both the tensile strength, σ_U, and the ultimate tensile strain, ε_U, predicted by $CNB + \tau^*$.

Table 8: Comparison of the tensile strength obtained by experiments, $CNB + \tau^*$, Neumeister and SFF

Material	$\sigma_{U_{Experimental}}$ (MPa)	$\sigma_{U_{CNB+\tau^*}}$ (MPa)	$\sigma_{U_{Neumeister}}$ (MPa)	$\sigma_{U_{SFF}}$ (MPa)
T700SC	1055.00	1067.28	1377.44	1365.20
AS400	1890.00	183.12	2710.59	2293.57
AS-4	1890.00	1939.22	3097.11	2623.79
Glass	940.00	940.02	940.29	397.93
L2 relative error norm		**2.45%**	**34.06%**	**27.52%**

4 CONCLUSIONS

A fragmentation model for the tensile response of unidirectional composites was developed in the present work. The model is the combination of two developments: 1) the previously published CNB model, which is based on the Neumeister model and allows obtaining an accurate ultimate tensile strength for CFRP and GFRP composites in terms of the number of fiber breaks per unit length, Λ, 2) A numerical procedure developed here to estimate the corrected fiber-matrix interfacial strength, τ^*, that 'contracts' the σ vs ε curve, in order to achieve a good agreement between the peak point of that curve and the strength predicted by CNB. This does not affect the stiffness of the material in the linear elastic zone, keeping constant the Young modulus. The present model is named $CNB + \tau^*$ model.

The accuracy of the $CNB + \tau^*$ model was evaluated by comparing the ultimate tensile strengths obtained by the model with the experimental ones reported in literature for four composite systems. According to the results, this initial assessment shows that $CNB + \tau^*$ model is more accurate than other GLS-based analytical models (Neumeister and SFF). Results show that the strength obtained by $CNB + \tau^*$ is lower than the one found by Neumeister for all composites systems considered here, with more important differences for the carbon-reinforced composites than for the glass-reinforced one. On the other hand, the tensile strength predicted by SFF can be lower or higher than the one obtained by $CNB + \tau^*$. It is important to highlight that the critical density of fibers breaks, Λ_C, which corresponds to the ultimate tensile strength of the composite, is larger in the $CNB + \tau^*$ than in the original Neumeister model, and this is attributable to the decrease of the average length of the fiber fragments with the reduction of the fiber-matrix interfacial strength.

The $CNB + \tau^*$ model was used to study the influence of the fiber content, V_f, on the stress-strain response of four composite systems by means of novel mechanical-performance maps. The principal conclusions can be summarized as follows:

- As reasonable, the increase of the ultimate tensile strength, σ_u, with V_f is predicted by the model, but this increase is dissimilar between CFRP and GFRP composites; in the first case, it is non-linear, in the second one, it can be considered linear.
- Generally speaking, the behavior of the ultimate strain, ε_U, with the fiber content, V_f, is not monotonous for the CFRP composites, whereas an increasing non-linear behavior was found for the GFRP one. Two aspects were identified to govern this: the reduction of the strain with V_f in the elastic zone for a given stress, and the influence of V_f on the development of the fiber fragmentation phenomenon. The second aspect is in turn determined by the stress concentration around the broken fibers and the damage progression in a transverse plane. According to the results, the reduction of the probability to obtain a determined number of fiber breaks in a transverse plane with the increase of V_f, which leads to the reduction of the damage probability before reaching a determined deformation, is the predominant effect for the GFRP composite. For the CFRP composites, a predominant effect for all fiber contents, V_f, is not identified.
- The change of the total strain energy, U_T, with V_f is non-monotonous and non-linear for the CFRP composites, whereas for the GFRP composite, it is linear increasing. According to the results, two opposite effects shall be considered to analyze the behavior of the fracture toughness with V_f: the increase of the Young modulus and ultimate tensile strength with V_f, and the increase of the stress concentration factor around the fiber breaks with V_f. The first effect seems to be predominant for the GFRP composite, while for the CFRP composites, a major effect is not manifested for all fiber contents, V_f.
- For a determined composite system, the percent contributions of the linear elastic zone (IF) and fragmentation zone (FM) to the total energy released during the damage process are almost invariant with the fiber content, V_f. For the

four composite systems considered here, the energy released in the FM zone is larger than the one released in the IF zone, and this difference is bigger for the GFRP composite.

ACKNOWLEDGMENTS

This work was supported by Administrative Department of Science, Technology and Innovation, Colciencias (Colombia) [grant number 1210-669-46014]; Polymers Laboratory of Instituto Tecnológico Metropolitano, Medellín (Colombia); Enlazamundos, Agencia Superior de Medellín, (Colombia) [grant year 2015]. The financial support of the Institución Universitaria Pascual Bravo (IUPB) is gratefully acknowledged as well.

Author's Contributions: Conceptualization, JD Vanegas and ID Patiño; Formal analysis, JD Vanegas and ID Patiño; Methodology, JD Vanegas and ID Patiño; Investigation, JD Vanegas and ID Patiño; Writing - original draft, .D Vanegas and ID Patiño; Writing - review & editing, JD Vanegas and ID Patiño; Software, JD Vanegas and ID Patiño; Validation, JD Vanegas and ID Patiño.

Editor: Pablo Andrés Muñoz Rojas.

References

Ali, Mohammad Irshad and J. Anjaneyulu. 2018. "Effect of Fiber-Matrix Volume Fraction and Fiber Orientation on the Design of Composite Suspension System." *IOP Conference Series: Materials Science and Engineering* 455(1):1–11.

Angelo, Marcus Vinícius, Marcelo Leite Ribeiro, and Volnei Tita. 2018. "A Computational Framework for Predicting Onset and Crack Propagation in Composite Structures via EXtended Finite Element Method (XFEM)." *Latin American Journal of Solids and Structures* 15(11):1–14.

Augusto, Fabián. 2019. "Two-Dimensional Numerical Model of the Fracture Process in Steel Fibre Reinforced Concrete with the Continuum Strong Discontinuity Approach and Functional Data Analysis." *Latin American Journal of Solids and Structures* 16(4):1–24.

Behzadi, Shabnam, Paul T. Curtis, and Frank R. Jones. 2009. "Improving the Prediction of Tensile Failure in Unidirectional Fibre Composites by Introducing Matrix Shear Yielding." *Composites Science and Technology* 69(14):2421–27.

Beyerlein, Irene J. and S. Leigh Phoenix. 1996a. "Statistics for the Strength and Size Effects of Microcomposites with Four Carbon Fibers in Epoxy Resin." *Composites Science and Technology* 56(1):75–92.

Beyerlein, Irene J. and S. Leigh Phoenix. 1996b. "Stress Concentrations around Multiple Fiber Breaks in an Elastic Matrix with Local Yielding or Debonding Using Quadratic Influence Superposition." *Journal of the Mechanics and Physics of Solids* 44(12):1997–2036.

Bijwe, Jayashree and Rekha Rattan. 2007. "Carbon Fabric Reinforced Polyetherimide Composites: Optimization of Fabric Content for Best Combination of Strength and Adhesive Wear Performance." *Wear* 262:749–58.

Bunsell, Anthony, Larissa Gorbatikh, Hannah Morton, Soraia Pimenta, Ian Sinclair, Mark Spearing, Yentl Swolfs, and Alain Thionnet. 2018. "Benchmarking of Strength Models for Unidirectional Composites under Longitudinal Tension." *Composites Part A: Applied Science and Manufacturing* 111(December 2017):138–50.

Chang, Y. S., J. J. Lesko, S. W. Case, D. A. Dillard, and K. L. Reifsnider. 1994. "The Effect of Fiber-Matrix Interphase Properties on the Quasi-Static Performance of Thermoplastic Composites." *Journal of Thermoplastic Composite Materials* 7(4):311–24.

Chen, Nian Zhong and C. Guedes Soares. 2007. "Progressive Failure Analysis for Prediction of Post-Buckling Compressive Strength of Laminated Composite Plates and Stiffened Panels." *Journal of Reinforced Plastics and Composites* 26(10):1021–42.

Curtin, William A. 1991a. "Exact Theory of Fibre Fragmentation in a Single-Filament Composite." *Journal of Materials Science & Technology* 26(1991):5239–53.

Curtin, William A. 1991b. "Theory of Mechanical Properties of Ceramic-Matrix Composites." *Journal of the American Ceramic Society* 74(11):2837–45.

Curtin, William A. 2000. “Tensile Strength of Fiber-Reinforced Composites: III. Beyond the Traditional Weibull Model for Fiber Strengths.” *Journal of Composite Materials* 34(15):1301–32.

Curtin, William A. and N. Takeda. 1998a. “Tensile Strength of Fiber-Reinforced Composites: I. Mode and Effects of Local Fiber Geometry.” *Journal of Composite Materials* 32(22):2042–59.

Curtin, William A. and N. Takeda. 1998b. “Tensile Strength of Fiber-Reinforced Composites: II. Application to Polymer Matrix Composites.” *Journal of Composite Materials* 32(22):2060–81.

DeMorais, A. B. 2006. “Prediction of the Longitudinal Tensile Strength of Polymer Matrix Composites.” *Composites Science and Technology* 66:2990–96.

Diao, H., A. Bismarck, P. Robinson, and Michael R. Wisnom. 2014. “Production of Continuous Intermingled CF/GF Hybrid Composite via Fibre Tow Spreading Technology.” P. 8 in *ECCM16 - 16TH EUROPEAN CONFERENCE ON COMPOSITE MATERIALS*. Sevilla.

Feih, Stefanie, Karen Wonsyld, Daniel Minzari, Peter Westermann, and Hans Lilholt. 2004. *Testing Procedure for the Single Fiber Fragmentation Test.* Vol. 1483. Roskilde.

Friedrich, Leandro Ferreira and Chong Wang. 2016. “Continuous Modeling Technique of Fiber Pullout from a Cement Matrix with Different Interface Mechanical Properties Using Finite Element Program.” *Latin American Journal of Solids and Structures* 13(10):1937–53.

Fukuda, Hiroshi and Tomonori Miyazawa. 1994. “Micromechanical Approach to the Tensile Strength of Unidirectional Composites.” *Advanced Composite Materials* 4(2):101–10.

Gaur, Umesh and Bernard Miller. 1989. “Microbond Method for Determination of the Shear Strength of a Fiber/Resin Interface: Evaluation of Experimental Parameters.” *Composites Science and Technology* 34(1):35–51.

Ghannadpour, S. A. M. and M. Shakeri. 2018. “Energy Based Collocation Method to Predict Progressive Damage Behavior of Imperfect Composite Plates under Compression.” *Latin American Journal of Solids and Structures* 15(4).

Gillich, Gilbert Rainer, Nuno M. M. Maia, Ion Cornel Mituletu, Marius Tufoi, Vasile Iancu, and Zoltan Korka. 2016. “A New Approach for Severity Estimation of Transversal Cracks in Multi-Layered Beams.” *Latin American Journal of Solids and Structures* 13(8):1526–44.

Harlow, D. G. and S. L. Phoenix. 1978a. “The Chain-of-Bundles Probability Model For the Strength of Fibrous Materials I: Analysis and Conjectures.” *Journal of Composite Materials* 12(2):195–214.

Harlow, D. G. and S. L. Phoenix. 1978b. “The Chain-of-Bundles Probability Model For the Strength of Fibrous Materials II: A Numerical Sudy of Converfence.” *Journal of Composite Materials* 12(2):195–214.

Hui, C. Y., S. Leigh Phoenix, M. Ibnabdeljalilt, and R. L. Smiths. 1995. “An Exact Closed Form Solution for Fragmentation of Weibull Fibers in a Single Filament Composite with Applications to Fiber-Reinforced Ceramics.” *Journal of the Mechanics and Physics of Solids* 43(10):1551–85.

Ibnabdeljalil, M. and William A. Curtin. 1997. “Strength and Reliability of Fiber-Reinforced Composites: Localized Load-Sharing and Associated Size Effects.” *International Journal of Solids and Structures* 34(21):2649–68.

Koyanagi, Jun, Hiroshi Hatta, Masaki Kotani, and Hiroyuki Kawada. 2009. “A Comprehensive Model for Determining Tensile Strengths of Various Unidirectional Composites.” *Journal of Composite Materials* 43(18):1901–14.

Lamon, Jacques. 2010. “Stochastic Models of Fragmentation of Brittle Fibers or Matrix in Composites.” *Composites Science and Technology* 70(5):743–51.

Landis, Chad M., Irene J. Beyerlein, and Robert M. McMeeking. 2000. “Micromechanical Simulation of the Failure of Fiber Reinforced Composites.” *Journal of the Mechanics and Physics of Solids* 48:621–48.

Lee, Nam-jeong and Jyongsik Jang. 1999. “The Effect of Fibre Content on the Mechanical Properties of Glass Fibre Mat / Polypropylene Composites.” *Composites Part A* 30:815–22.

Li, J. 2010. “The Effect of Carbon Fiber Content on the Mechanical and Tribological Properties of Carbon Fiber-Reinforced PTFE Composites.” *Polymer - Plastics Technology and Engineering* 49:332–36.

Liu, Xiaokang, Binbin Yang, Longsheng Lu, Zhenping Wan, and Yong Tang. 2018. “A Thermoplastic Multilayered Carbon-Fabric/Polycarbonate Laminate Prepared by a Two-Step Hot-Press Technique.” *Polymers* 10(7):1–17.

Madhukar, Madhu S. and Lawrence T. Drzal. 1991. “Fiber-Matrix Adhesion and Its Effect on Composite Mechanical Properties: II. Longitudinal (0°) and Transverse (90°) Tensile and Flexure Behavior of Graphite/Epoxy Composites.” *Journal of Composite Materials* 25(8):958–91.

Matveev, M. Y., a. C. Long, and I. a. Jones. 2014. “Modelling of Textile Composites with Fibre Strength Variability.” *Composites Science and Technology* 105:44–50.

Mazen, A., M. Metwalli, and N. El-Mahallawy. 2007. “Tensile Deformation Behavior of Epoxy Composites Reinforced With Three Different Woven Fabrics.” *International Conference on Aerospace Sciences and Aviation Technology* 12(ASAT CONFERENCE):1–17.

Morshedsolouk, Fattaneh and Mohammad Reza Khedmati. 2014. “Parametric Study on Average Stress–Average Strain Curve of Composite Stiffened Plates Using Progressive Failure Method.” *Latin American Journal of Solids and Structures* 11(12):2203–26.

Na, Wonjin, Geunsung Lee, Minchang Sung, Heung Nam Han, and Woong Ryeol Yu. 2017. “Prediction of the Tensile Strength of Unidirectional Carbon Fiber Composites Considering the Interfacial Shear Strength.” *Composite Structures* 168:92–103.

Naranjo-Lozada, Juan, Horacio Ahuett-Garza, Pedro Orta-Castañón, Wilco M. H. Verbeeten, and Daniel Sáiz-González. 2019. “Tensile Properties and Failure Behavior of Chopped and Continuous Carbon Fiber Composites Produced by Additive Manufacturing.” *Additive Manufacturing* 26:227–41.

Neumeister, Jonas M. 1993a. “A Constitutive Law for Continuous Fiber Reinforced Brittle Matrix Composites with Fiber Fragmentation and Stress Recovery.” *Journal of the Mechanics and Physics of Solids* 41(8):1383–1404.

Neumeister, Jonas M. 1993b. “Bundle Pullout—a Failure Mechanism Limiting the Tensile Strength of Continuous Fiber Reinforced Brittle Matrix Composites— and Its Implications for Strength Dependence on Volume and Type of Loading.” *Journal of the Mechanics and Physics of Solids* 41(8):1405–24.

Ohsawa, T., A. Nakayama, M. Miwa, and A. Hasegawa. 1978. “Temperature Dependence of Critical Fiber Length for Glass Fiber-Reinforced Thermosetting Resins.” *Journal of Applied Polymer Science* 31:3203–12.

Okabe, Tomonaga, N. Takeda, Y. Kamoshida, M. Shimizu, and William A. Curtin. 2001. “A 3D Shear-Lag Model Considering Micro-Damage and Statistical Strength Prediction of Unidirectional Fiber-Reinforced Composites.” *Composites Science and Technology* 61(12):1773–87.

Rochardjo, Heru S. B., Jun Komotori, Masao Shimizua, and Yasushi Miyano. 1997. “Effects of the Fiber Content on the Longitudinal Tensile Fracture Behavior of Uni-Directional Carbon/Epoxy Composites.” *Journal of Materials Processing Technology* 67:89–93.

Sastry, a. M. and S. Leigh Phoenix. 1993. “Load Redistribution near Non-Aligned Fibre Breaks in a Two-Dimensional Unidirectional Composite Using Break-Influence Superposition.” *Journal of Materials Science Letters* 12(20):1596–99.

Swolfs, Yentl, R. M. McMeeking, V. P. Rajan, F. W. Zok, Ignaas Verpoest, and Larissa Gorbatikh. 2015. “Global Load-Sharing Model for Unidirectional Hybrid Fibre-Reinforced Composites.” *Journal of the Mechanics and Physics of Solids* JMPSD1400292.

Turon, Albert, J. Costa, P. Maimí, D. Trias, and J. A. Mayugo. 2005. “A Progressive Damage Model for Unidirectional Fibre-Reinforced Composites Based on Fibre Fragmentation. Part I: Formulation.” *Composites Science and Technology* 65(13):2039–48.

Vanegas-Jaramillo, J. D., A. Turon, J. Costa, L. J. Cruz, and J. A. Mayugo. 2018. “Analytical Model for Predicting the Tensile Strength of Unidirectional Composites Based on the Density of Fiber Breaks.” *Composites Part B: Engineering* 141(November 2017):84–91.

Vanegas-jaramillo, Juan D., Iván D. Patiño-Arcila, and Carlos A. Vargas-Isaza. 2013. “Vacíos Por Atrapamiento Mecánico En Procesos de Moldeo Líquido : Mecanismo de Formación, Influencia En El Comportamiento Mecánico y Reducción.” *Tecnológicas* (30):149–81.

Wagner, W. and C. Balzani. 2010. “Prediction of the Postbuckling Response of Composite Airframe Panels Including Ply Failure.” *Engineering Fracture Mechanics* 77(18):3648–57.

Wang, Chong and Leandro Ferreira Friedrich. 2013. “Computational Model of Spalling and Effective Fibers on Toughening in Fiber Reinforced Composites at an Early Stage of Crack Formation.” *Latin American Journal of Solids and Structures* 10(4):797–811.

Watanabe, J., F. Tanaka, H. Okuda, and Tomonaga Okabe. 2014. “Tensile Strength Distribution of Carbon Fibers at Short Gauge Lengths.” *Advanced Composite Materials* 23(5–6):535–50.

Yang, Binbin, Longsheng Lu, Xiaokang Liu, Yingxi Xie, Jingwen Li, and Yong Tang. 2017. “Uniaxial Tensile and Impact Investigation of Carbon-Fabric/Polycarbonate Composites with Different Weave Tow Widths.” *Materials and Design* 131:470–80.

Yu, Tianyu, Ziyang Zhang, Shutao Song, Yuanli Bai, and Dazhong Wu. 2019. “Tensile and Flexural Behaviors of Additively Manufactured Continuous Carbon Fiber-Reinforced Polymer Composites.” *Composite Structures* In press:1–18.

Zhandarov, Serge and Edith Mäder. 2014. “An Alternative Method of Determining the Local Interfacial Shear Strength from Force-Displacement Curves in the Pull-out and Microbond Tests.” *International Journal of Adhesion and Adhesives* 55:37–42.

Zhang, Zhifeng, Haoran Chen, and Lin Ye. 2008. “Progressive Failure Analysis for Advanced Grid Stiffened Composite Plates/Shells.” *Composite Structures* 86(1–3):45–54.

Zhou, S. J. and William A. Curtin. 1995. “Failure of Fiber Composites: A Lattice Green Function Model.” *Acta Metallurgica et Materialia* 43(8):3093–3104.

Zhou, Yuanxin, Mohammed a. Baseer, Hassan Mahfuz, and Shaik Jeelani. 2006. “Statistical Analysis on the Fatigue Strength Distribution of T700 Carbon Fiber.” *Composites Science and Technology* 66(13):2100–2106.